European Journal of Medicinal Chemistry 277 (2024) 116737

Contents lists available at ScienceDirect

European Journal of Medicinal Chemistry

journal homepage: www.elsevier.com/locate/ejmech

Research paper

Optimization of potent, broad-spectrum, and specific anti-influenza compounds targeting RNA polymerase PA-PB1 heterodimerization

Anna Bonomini [a,2], Tommaso Felicetti [b,2], Martina Pacetti [b], Chiara Bertagnin [a], Alice Coletti [b], Federica Giammarino [c], Marta De Angelis [d], Federica Poggialini [e], Antonio Macchiarulo [b], Stefano Sabatini [b], Beatrice Mercorelli [a], Lucia Nencioni [d], Ilaria Vicenti [c], Elena Dreassi [e], Violetta Cecchetti [b], Oriana Tabarrini [b], Arianna Loregian [a,**,1], Serena Massari [b,*,1]

[a] Department of Molecular Medicine, University of Padua, 35121, Padua, Italy
[b] Department of Pharmaceutical Sciences, University of Perugia, 06123, Perugia, Italy
[c] Department of Medical Biotechnologies, University of Siena, 53100, Siena, Italy
[d] Department of Public Health and Infectious Diseases, Laboratory Affiliated to Istituto Pasteur Italia-Fondazione Cenci Bolognetti, Sapienza University of Rome, 00185, Rome, Italy
[e] Department of Biotechnology, Chemistry and Pharmacy, University of Siena, 53100, Siena, Italy

A B S T R A C T

Influenza viruses (IV) are single-stranded RNA viruses with a negative-sense genome and have the potential to cause pandemics. While vaccines exist for influenza, their protection is only partial. Additionally, there is only a limited number of approved anti-IV drugs, which are associated to emergence of drug resistance. To address these issues, for years we have focused on the development of small-molecules that can interfere with the heterodimerization of PA and PB1 subunits of the IV RNA-dependent RNA polymerase (RdRP). In this study, starting from a cycloheptathiophene-3-carboxamide compound that we recently identified, we performed iterative cycles of medicinal chemistry optimization that led to the identification of compounds **43** and **45** with activity in the nanomolar range against circulating A and B strains of IV. Mechanistic studies demonstrated the ability of **43** and **45** to interfere with viral RdRP activity by disrupting PA-PB1 subunits heterodimerization and to bind to the PA C-terminal domain through biophysical assays. Most important, ADME studies of **45** also showed an improvement in the pharmacokinetic profile with respect to the starting hit.

1. Introduction

In the past two decades, anthropogenic, climatic, demographic, and technological changes have altered the landscape of infectious diseases risk, creating the conditions for epidemics to thrive and grow [1]. Emerging infectious diseases have caused numerous outbreaks, severe illnesses, and many deaths. Along with HIV-1 and Severe Acute Respiratory Syndrome Coronavirus-2 (SARS-CoV-2), influenza A virus (IAV) is one of the RNA viruses that have posed the greatest threat to worldwide Public Health reaching also pandemic proportions. One of the primary targets for pandemic prevention and preparedness is the development of vaccines and therapeutics [2,3].

In this context, our group has been working for years in discovery of next-generation anti-IV agents, with a focus on the identification of small molecules able to interfere with IV RNA-dependent RNA polymerase (RdRP) PA-PB1 subunits heterodimerization. This innovative antiviral approach is supported by three main strengths.

The first strength is based precisely on RdRP, which has been largely validated as an attractive antiviral drug target [4–9]. It is essential for viral transcription and replication, its structure is highly conserved among all the IV strains, and no homolog has been found in mammalian cells [10–13]. The high profile of the RdRP as an antiviral drug-target was confirmed by the approval of inhibitors [14], such as the nucleoside analog **favipiravir** (**FPV**) (**T-705 or avigan®**) [15] that was approved in 2014 in Japan and the PA cap-dependent endonuclease inhibitor **baloxavir marboxil** [16] that was approved in 2018 in both Japan and the USA, and in 2021 also in Europe.

The second strength is the protein-protein interaction (PPI)

* Corresponding author. Department of Pharmaceutical Sciences, University of Perugia, 06123, Perugia, Italy.
** Corresponding author. Department of Molecular Medicine, University of Padua, 35121, Padua, Italy.
E-mail addresses: arianna.loregian@unipd.it (A. Loregian), serena.massari@unipg.it (S. Massari).
[1] Co-last authors.
[2] Co-first authors.

https://doi.org/10.1016/j.ejmech.2024.116737
Received 24 June 2024; Received in revised form 30 July 2024; Accepted 1 August 2024
Available online 3 August 2024

inhibition approach. In recent years, different studies have highlighted viral-viral or host-viral PPIs as valid drug-targets that could be exploited for the discovery of alternative antiviral drugs [17–19]. The IV RdRP is a heterotrimer formed by three proteins, polymerase basic 1 (PB1), polymerase basic 2 (PB2), and polymerase acidic (PA), which establish numerous PPIs. Indeed, RdRP subunits are stably bound, in a head-to-tail fashion, through extensive interactions mainly between the PB1 N-terminal ($PB1_N$) and the PA C-terminal (PA_C), and the PB1 C-terminal ($PB1_C$) and the PB2 N-terminal ($PB2_N$). On the basis of the essential role played by the heterotrimerization process for RdRP functions, the development of RdRP subunits interaction inhibitors has been proven to be a valid and alternative approach to interfere with RdRP activity [20–22]. Additionally, RdRP subunits establish interactions with a number of host proteins that are essential cofactors for RdRP localization and functions [23–25], opening perspective of developing host-viral PPI inhibitors. PPIs by viral proteins are generally characterized by a high specificity and degree of conservation, and the requirement for the simultaneous mutation of at least one residue on both binding proteins to develop resistance. Thus, the main potential advantages of targeting PPIs are the achievement of an anti-IV agent endowed with a specific and broad-spectrum activity, as well as a high barrier to drug-resistance, thus overcoming the main limitations that characterize the currently available drugs. Indeed, with the exception of **FPV**, which induces lethal viral mutagenesis, the development of resistance has been determined in patients for all approved anti-IV drugs, including **baloxavir marboxil**. In particular, viruses containing PA/I38X substitutions were identified in **baloxavir**-treated patients, which was associated with transient rises in infectious virus titers, prolongation of virus detectability, and initial delay in symptoms alleviation [26].

The third strength concerns the peculiar features of PA-PB1 subunits interaction. Some PPIs between RdRP subunits have been already demonstrated to be druggable and, among them, main research efforts have been devoted to the discovery of PA-PB1 interaction inhibitors [20,27]. Two crystal structures of the PA_C-$PB1_N$ interface have been reported in 2008 [28,29]. Both crystal structures showed that subunits' binding is driven by relatively few residues, suggesting the feasibility of using small molecules to interfere with PA-PB1 interaction. Moreover, the first 15 $PB1_N$ residues involved in the PA_C binding are highly conserved among avian and human IV strains [30]. Finally, mutations deliberately introduced into the PA_C or $PB1_N$ termini resulted into a limited ability of IV to compensate [31].

These findings prompted the search for PA-PB1 heterodimerization inhibitors, and, since 2012, different chemical classes of compounds have been reported in literature (Fig. 1), such as 1,2,4-triazolopyrimidines (compounds **1–3**) [32–34], benzoimidazol-2-ones (compound **4**) [35], octahydronaphthalen-1-ones (compound **5**) [36], and quinolin-2-ones (compound **6**) [37]. The first compounds to be reported were characterized by an anti-IV activity in the micromolar range, which was increased over time thanks to their chemical optimization. Of note, the optimization study performed on quinolin-2-one derivatives led the to the identification of compound **6**, one of the most recent and potent anti-IV derivatives to be reported, showing an effective concentration at half-maximal response (EC_{50}) of 61 nM, albeit its ability to interfere with PA-PB1 heterodimerization was not reported.

For many years, our group has been working on the identification of small molecules able to interfere with RdRP functions through the inhibition of PA-PB1 heterodimerization. Starting from the cycloheptathiophene-3-carboxamide (cHTC) derivative **7** (Fig. 2), emerged from a virtual screening on the PA_C crystal structure [38], we undertook a first optimization phase that led to the identification of derivative **8** that exhibited an improved anti-PA-PB1 effect (IC_{50} = 32 μM) and, most importantly, acquired anti-IV activity (EC_{50} = 18 μM) at non-toxic concentrations (CC_{50} > 250 μM) [39]. Then, a second optimization phase afforded five compounds (**9–13**, Fig. 2) endowed with potent antiviral activity against IAV/PR/8/34 (PR8) strain (EC_{50s} = 0.23–2.1 μM) and a broad-spectrum potential when tested against additional IAV and IBV strains (plaque reduction assay [PRA], MDCK cells) [40,41]. Compounds were also potent inhibitors of IV RdRP activity (IC_{50s} = 0.27–2.8 μM, minireplicon assay) and strong PA-PB1 heterodimerization disruptors (IC_{50s} = 5.2–15 μM, ELISA), with the exception of compound **10** (IC_{50} = 81 μM). However, the main issue of these compounds relies on a very low water solubility that strongly undermines further in-depth studies and their potential for development.

Therefore, in this study, an additional medicinal chemistry optimization was performed to explore SAR as well as to improve anti-IV activity and pharmacokinetic profile of cHTC derivatives. Initially, starting

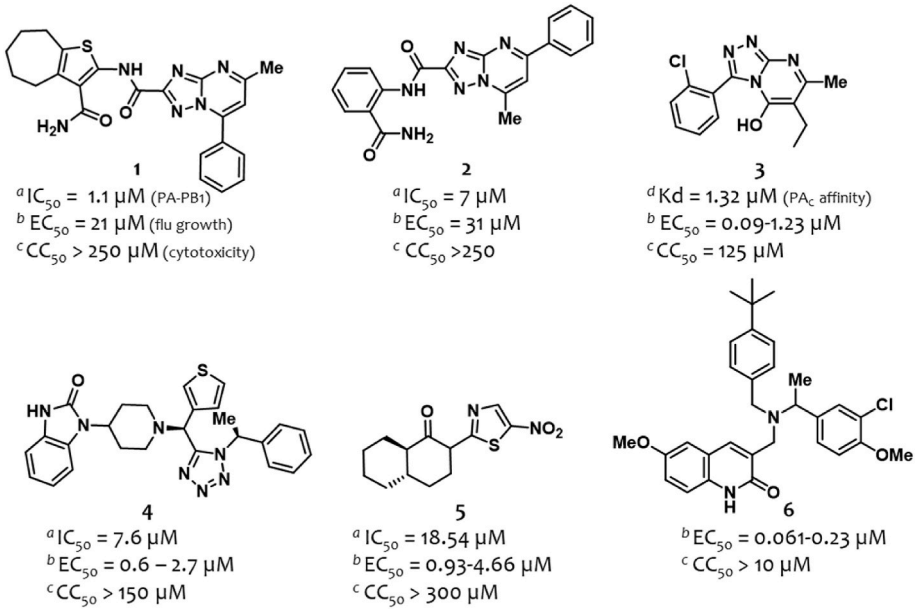

Fig. 1. Structure and biological activities of PA-PB1 heterodimerization inhibitors **1–6** previously reported. [a] The IC_{50} value represents the compound concentration that reduces the PA-PB1 complex formation by 50 %; [b] the EC_{50} value represents the compound concentration that inhibits 50 % of IV replication; [c] the CC_{50} value represents the compound concentration that inhibits 50 % of cell viability; [d] the K_d value represents the dissociation constant of compound with the PA_C.

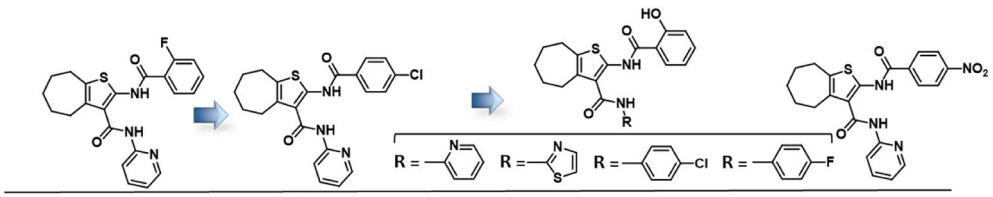

	7	8	9	10	11	12	13
[a] IC_{50} (PA-PB1)	90 μM	32 μM	15 μM	81 μM	15 μM	5.2 μM	6.0 μM
[b] EC_{50} (flu growth)	> 100 μM	18 μM	2.1 μM	0.24 μM	1.2 μM	0.88 μM	0.23 μM
[c] IC_{50} (RdRP activity)	> 100 μM	10 μM	2.8 μM	0.33 μM	1.0 μM	0.47 μM	0.27 μM
[d] CC_{50} (cytotoxicity)	> 250 μM	>250 μM	>250 μM	>250 μM	>250 μM	>250 μM	>250 μM
[e] SI (selectivity index)		>14	>119	>1041	>208	>284	>1086

Fig. 2. Structure and biological activities of cHTC compounds **7–13** previously reported. For the definition of [a] IC_{50}, [b] EC_{50}, and [d] CC_{50}, see Table 1 caption; [c] the IC_{50} value represents the compound concentration that reduces by 50 % the activity of IAV RNA polymerase; [e] SI (selectivity index) represents the ratio between CC_{50} and EC_{50} values.

from compound **13**, two series of analogs were designed and synthesized (Fig. 3), by extensively modifying the substituents at the C-3 (compounds **14–22**) and C-2 (compounds **23–32**) positions of the core. Then, based on the obtained results and previous SAR insights, a third series was finely designed by combining the best moieties emerged as C-2 and C-3 substituents, leading to compounds **33–46** (Fig. 3). The study led to the identification of very potent anti-IV agents, with some compounds active in the nanomolar range. In-depth studies focused on two of the most promising analogs (compounds **43** and **45**) highlighted potent, broad spectrum, and specific anti-IV activity accomplished by potent ability to disrupt PA-PB1 subunits heterodimerization and to interfere with viral RdRP activity. Finally, completing our starting aims, compound **45** showed a significant increase in water solubility with respect to hit compound **13**, coupled with promising stability in the presence of microsomes and plasma enzymes.

2. Results and discussion

2.1. Chemistry

The synthesis of C-3 functionalized cHTC derivatives **14–22** started, as outlined in Scheme 1, by preparing 2-cyano-*N*-(substituted) acetamide compounds **48** [40], **49** [40], **50** [40], **51**–**54**, and **56** *via* reaction of 3-(3,5-dimethyl-1*H*-pyrazol-1-yl)-3-oxopropanenitrile **47** [42] with appropriate amines in toluene. Derivative **47** [42] was prepared, as reported in literature, by reacting ethyl 2-cyanoacetate with hydrazine monohydrate, followed by the reaction with acetylacetone. Derivatives **48–56** were then used in the successive two-steps Gewald reaction, entailing an initial Knoevenagel condensation with cycloheptanone, furnishing α,β-unsaturated nitrile intermediates, which were used without isolation in the successive cyclization step. Cyclization was performed in the presence of sulfur and *N*,*N*-diethylamine in EtOH, to give intermediates **57** [40], **58** [40], **59** [40], **60**, **61** [43], **62**, **63**, **64** [44], and **65** [44]. The successive C-2 amidation, accomplished by reacting compounds **57–65** with 4-nitrobenzoyl chloride in dry pyridine, furnished target compounds **14–21** and methoxyl intermediate **66**. Finally, *O*-demethylation of methoxyl intermediate **66** in the presence of BBr_3 in dry CH_2Cl_2 yielded 2-hydroxyl target derivate **22**.

As outlined in Scheme 2, the synthesis of C-2 functionalized cHTC derivatives **23–25** and **27–32** entailed the preparation of key intermediate **68** [39] using the two-steps Gewald reaction. Thus, the Knoevenagel condensation of cycloheptanone with 2-cyano-*N*-pyridin-2-ylacetamide **67** [42], which was in turn synthesized by reacting compound **47** [42] with 2-aminopyridine in toluene, furnished α,β-unsaturated nitrile that was cyclized to give intermediate **68**. Then, the successive coupling reaction of compound **68** with the appropriate acyl chlorides in dry pyridine yielded target compounds **23–25**, **27**, **28**, and **30–32**, and methoxyl intermediate **69**. *O*-demethylation reaction of compound **69** performed with BBr_3 in dry CH_2Cl_2 provided the 2-hydroxyl target compound **29**.

Finally, as reported in Scheme 3, C-2 amidation of intermediates **58** [40], **60** [43], **64** [40], and **65** [44] with the appropriate acyl chlorides

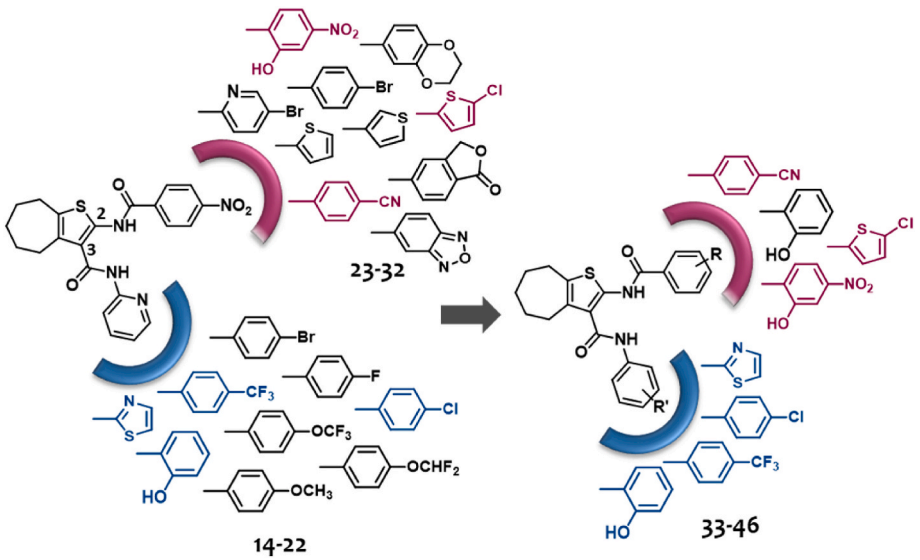

Fig. 3. Structure of cHTC derivatives **14–46** synthesized in this study.

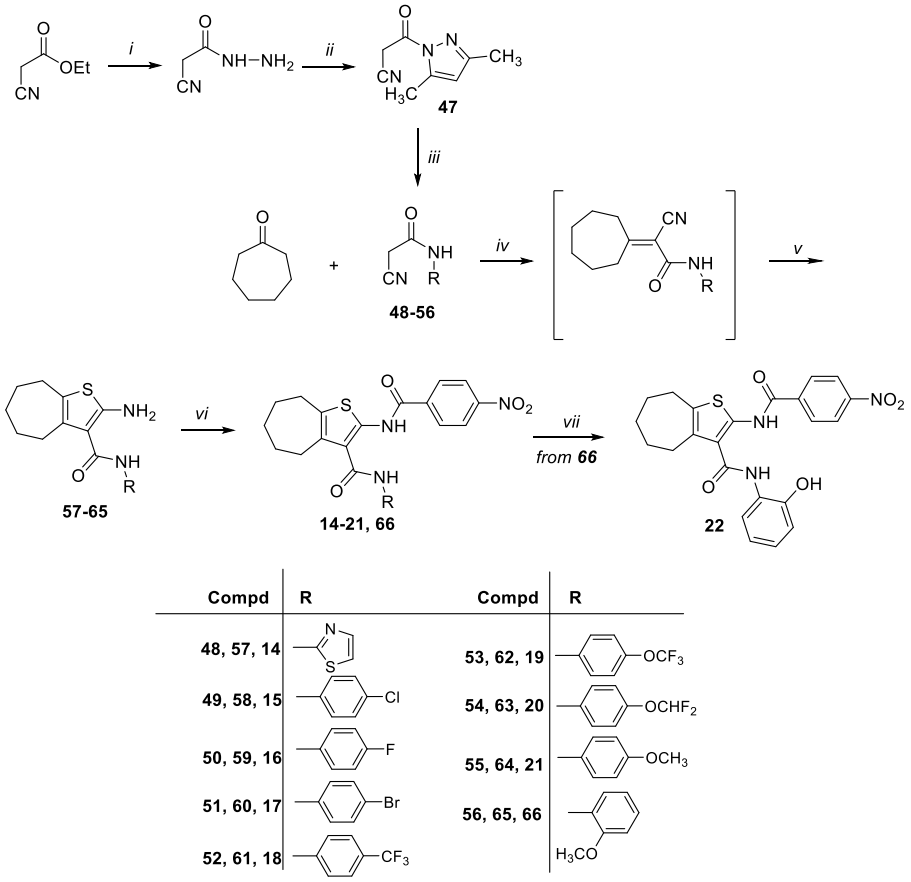

Scheme 1. [a] **Reagents and conditions:** (*i*) hydrazine monohydrate, rt; (*ii*) acetylacetone, H_2O, HCl 12N, rt; (*iii*) amines, toluene, reflux; (*iv*) cycloheptanone, ammonium acetate, glacial acetic acid, benzene, reflux; (*v*) sulfur, *N*,*N*-diethylamine, EtOH dry, 50 °C; (*vi*) 4-nitrobenzoyl chloride, dry pyridine, rt; (*vii*) BBr_3, dry CH_2Cl_2, from 0 °C to rt.

in dry pyridine yielded 4-benzonitrile derivatives **33**, **36**, and **40**, 5-chlorothiophene derivatives **35**, **39**, and **42**, and intermediates **70–77**. *O*-demethylation of intermediates **70–77** in the presence of BBr_3 in dry CH_2Cl_2 furnished target compounds **34**, **37**, **38**, **41**, and **43–46**.

2.2. Design of compounds *14–46* and their evaluation for anti-PA-PB1 heterodimerization and anti-IV activity

Starting from compound **13**, a first set of compounds (derivatives **14–22**, Fig. 3 and Table 1) was initially synthesized maintaining the 4-nitrophenyl ring at the C-2 position of the cHTC scaffold, while exploring different moieties as C-3 substituents.

Based on the SAR insight previously acquired, 1,3-thiazole, 4-chlorophenyl and 4-fluorophenyl rings, which emerged as the best substituents in the C-2 2-hydroxyphenyl series (compounds **10–12**, Fig. 2), were studied by synthesizing 4-nitrophenyl derivatives **14–16**, respectively. Then, the presence of halogens at the *para* position of the C-3 phenyl ring was studied in bromine derivative **17**, and fluorine compounds **18–20** characterized by a 4-trifluoromethyl, 4-trifluoromethoxy, and 4-difluoromethoxy moieties, respectively. A 4-methoxy group was also explored in compound **21**, while a 2-hydroxyl moiety, the only hydrophilic substituent to be exploited, characterized compound **22**.

The synthesized compounds were evaluated for the ability to inhibit the PA-PB1 subunits interaction (by an ELISA-based assay), using the $PB1_{1\text{-}15}$-Tat peptide as a positive control, and for the anti-IV activity in MDCK cells infected with IAV/PR/8/34 strain (PR8) (by PRA), using **ribavirin** (RBV) and **FPV** as positive controls. In parallel, the compounds were tested for the cytotoxicity (by MTT assays in MDCK cells), to exclude that the observed anti-IV activity might be due to toxic effects in the cells.

All the compounds were unable to interfere with PA-PB1 heterodimerization *in vitro* (Table 1). Nevertheless, except for 4-fluorophenyl compound **16** and 4-methoxyphenyl compound **21**, all the compounds displayed anti-IV activity. Best results were shown by compound **14** (EC_{50} = 0.19 μM), which confirmed the 1,3-thiazole as a suitable C-3 substituent, and, surprisingly, by 2-hydroxyphenyl compound **22** (EC_{50} = 0.38 μM), suggesting that a hydrophilic substituent at the *ortho* position of the C-3 phenyl ring imparted antiviral activity. Halogen-containing compounds **15** and **17–20** also provided good results, exhibiting anti-IV activity with EC_{50} values ranging from 1.0 to 4.6 μM. All the compounds resulted non-toxic up to 250 μM concentration, except for derivative **22** that showed mild cytotoxicity (CC_{50} = 73 μM).

In order to study the role of the substituent at the C-2 position of the cHTC scaffold, the 4-nitrophenyl ring of compound **13** was modified in a second set of compounds (derivatives **23–32**, Fig. 3 and Table 2), while maintaining unaltered the C-3 pyridine ring. In detail, the 4-nitrophenyl ring was replaced by a 4-bromo-2-pyridine, 4-bromophenyl, and 2,3-dihydrobenzo[*b*][1,4]dioxine ring in derivatives **23–25**, respectively, and by thiazole-based moieties in derivatives **26–28**. The presence of a 4-nitro group on the C-2 phenyl ring was also studied in presence of a 2-hydroxy group in compound **29**. Finally, derivatives **30–32** were synthesized by replacing the 4-nitrophenyl ring by bioisosteric moieties, such as 4-benzonitrile, 1,3-dihydroisobenzofurane, and benzo[*c*][1,2,5] oxadiazole rings, respectively. When evaluated for the ability to interfere with PA-PB1 heterodimerization, all the C-2 modified compounds resulted inactive or weakly active and most of them were also devoid of anti-IV activity. Nevertheless, 5-chlorothiophene compound **27**, 2-hydroxy-4-nitrophenyl compound **29**, and 4-benzonitrile compound **30**

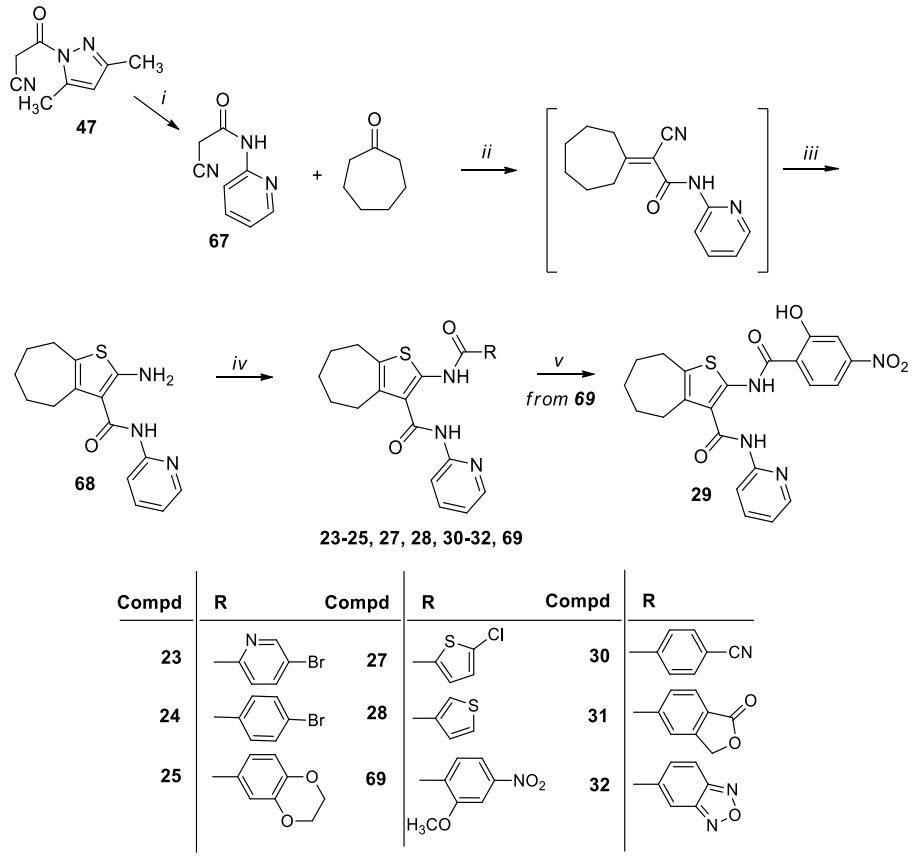

Compd	R	Compd	R	Compd	R
23		27		30	
24		28		31	
25		69		32	

Scheme 2. [a] **Reagents and conditions:** (*i*) 2-aminopyridine, toluene, reflux; (*ii*) ammonium acetate, glacial acetic acid, benzene, reflux; (*iii*) sulfur, *N*,*N*-diethylamine, EtOH, 50 °C; (*iv*) selected acyl chloride, dry pyridine, rt; (*v*) BBr_3, dry CH_2Cl_2, from 0 °C to rt.

exhibited good anti-IV activity with EC_{50} values of 1.0, 1.3, and 1.6 μM, respectively, at sub-cytotoxic concentrations (CC_{50} > 250, 188, and 141 μM, respectively).

Finally, the results obtained from the two series of compounds previously described and earlier SAR insights guided the design and synthesis of the last series of compounds. Thus, additional derivatives were synthesized (compounds **33–46**, Fig. 3 and Table 3) by combining the best moieties emerged as C-2 and C-3 substituents. In particular, the C-2 4-benzonitrile, 2-hydroxy-4-nitrophenyl, 5-chlorothiophene, and 2-hydroxyphenyl moieties were combined with each of the C-3 4-chlorophenyl, 4-trifluoromethylphenyl, 1,3-thiazole, and 2-hydroxyphenyl rings; within the C-2 2-hydroxyphenyl series, 1,3-thiazole and 4-chlorophenyl derivatives were not synthesized since being previously reported (compounds **10** and **11**, Fig. 2).

Among them, C-2 4-benzonitrile compounds **33** and **36**, 2-hydroxyphenyl compounds **37** and **44**, and 5-chlorothiohene derivatives **39**, **42**, and **46** were devoid of anti-PA-PB1 activity, but displayed potent anti-IV activity with EC_{50} values ranging from 0.085 μM to 1.8 μM at sub-cytotoxic concentrations. On the other hand, compounds **34**, **40**, and **41** showed the ability to disrupt PA-PB1 interaction (IC_{50} values of 17.3, 62.5, and 36.0 μM, respectively) but, unfortunately, we could not reliably test their activity by PRA, since these compounds exhibited low solubility in the dense cellulose-containing medium used in this assay. The same applied for the inactive compound **38**, which was also considerably cytotoxic (CC_{50} = 10 μM). These results might suggest that 2-hydroxy-4-nitrophenyl and 4-benzonitrile rings, characterizing compounds **34**, **38**, **40**, and **41**, were not suitable C-2 substituents. Nevertheless, their presence imparted to C-3 2-hydroxyphenyl compounds **43** and **45** the ability to interfere with both PA-PB1 heterodimerization *in vitro* and viral replication in infected cells. In particular, compounds **43** and **45** exhibited anti-PA-PB1 activity with IC_{50} values of 19.3 and 26.5 μM and anti-IV activity with EC_{50} values of 0.38 μM and 0.089 μM, respectively, at non-toxic concentrations (CC_{50} > 250 μM and 224 μM). Of note, with an EC_{50} of 85 and 89 nM, compounds **42** and **45** were the most potent anti-IV compounds herein synthesized and within the whole cHTC class of compounds, reaching SI values of >2,941 and 2,517, respectively. Compound **45** can be also counted as the most potent anti-IV compound reported so far acting by interfering with IV RdRP PA-PB1 subunit heterodimerization.

As shown in Tables 1–3, we observed a discrepancy between the activity *in vitro* and the activity in cellular assays for these compounds. Since dissociative compounds are expected to act in a competitive manner with one of the protein partners, the extent of their inhibitory effect (PA-PB1 disruption) depends on their affinity to the target, but also on the concentration of the target itself and on the experimental setting and the employed assay. As it is conceivable that the concentration of proteins used in the ELISA (hundreds of ng per well) may greatly exceed those produced in virus-infected cells, it is expected that compound concentrations required *in vitro* to achieve a given level of inhibition may be higher than those required to inhibit virus replication in the cellular context. This is in agreement with the IC_{50} of the PB1-derived peptide in the ELISA assay (Table 1) and with similar results described for dissociative compounds targeting other PPIs [45–47]. Nevertheless, the discrepancy between IC_{50} and EC_{50} values could also suggest an additional mechanism of action for cHTC compounds. Therefore, further studies were conducted to determine whether the anti-IV activity shown by the most potent compounds **43** and **45** was actually due to the ability to interfere with PA-PB1 heterodimerization.

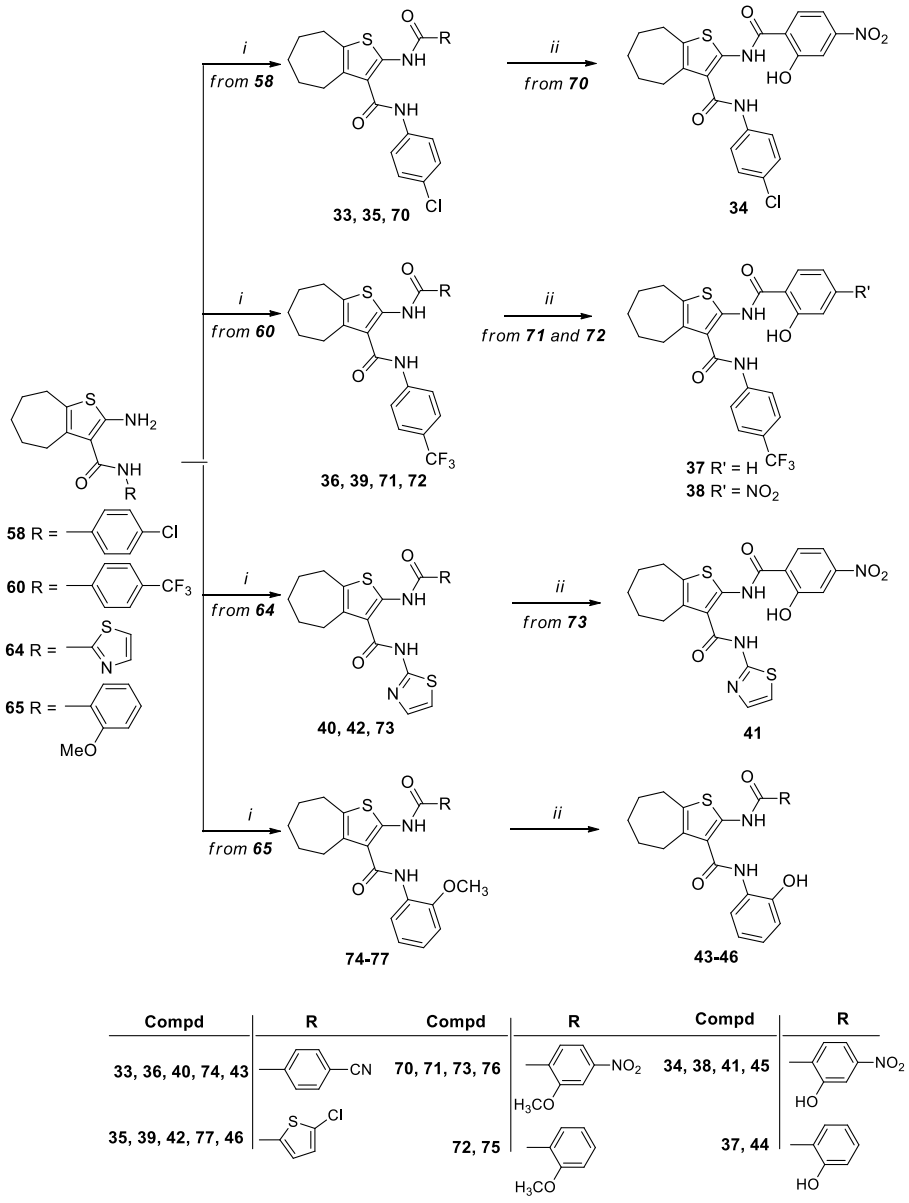

Scheme 3. [a] **Reagents and conditions:** (*i*) selected acyl chloride, dry pyridine, rt; (*ii*) BBr_3, dry CH_2Cl_2, from 0 °C to rt.

2.3. Compounds *43* and *45* inhibited the PA-PB1 heterodimerization in a cellular context

Accordingly, the first aim was to ascertain whether the best compounds **43** and **45** retained the ability to disrupt PA-PB1 heterodimerization in the cellular context. Compound **36** ($IC_{50} > 200$ μM and $EC_{50} = 1.8$ μM) was included as a negative control, being inactive in PA-PB1 ELISA-based assay. In particular, since PA and PB1 subunits enter the nucleus as a heterodimer (while PB2 enters the cell nucleus independently), we investigated whether compounds **36**, **43** and **45** could affect PA-PB1 binding in the cell cytoplasm by evaluating the intranuclear translocation of a PA-GFP fusion protein. Thus, we transfected HEK 293T cells with plasmids expressing PB1 and PA-GFP fusion protein and analyzed the intracellular localization of PA-GFP in the absence or in the presence of compounds **36**, **43**, and **45** (or DMSO as a control). As shown in Fig. 4, individually expressed PA-GFP was largely cytoplasmic, whereas co-expression of PA-GFP with PB1 resulted in marked nuclear accumulation of PA. Treatment of PA-PB1 co-expressing cells with compounds **43** and **45** impaired PA nuclear import, whereas compound **36** had no effect, similarly to DMSO (Fig. 4). These data demonstrated that, in accordance with the observations made in the cell-free ELISA, compounds **43** and **45** were able to interfere with PA-PB1 heterodimerization also in a cellular context.

2.4. Compounds *43* and *45* inhibited the activity of IAV RdRP in a minireplicon assay

Compounds able to displace the PA-PB1 interaction should lead to an interference with IAV RdRP activity in a cellular context. Therefore, compounds **43** and **45** were evaluated in a minireplicon assay at scalar concentrations. Compound **36** ($IC_{50} > 200$ μM and $EC_{50} = 1.8$ μM) was also included in this assay. Briefly, HEK 293T cells were co-transfected with plasmids encoding IAV nucleoprotein (NP), PA, PB1, and PB2 proteins, and the firefly luciferase RNA flanked by the noncoding regions of IAV/WSN/33 segment 8. Then, cells were treated with compounds **36**, **43**, and **45**, including RBV and **FPV** as positive controls. Intracellular reconstitution of functional vRNPs (in which all four PA, PB1, and PB2, and NP proteins are co-expressed and interact with each other) and consequent RNA synthesis were detected by measuring the expression of the firefly reporter gene. In parallel, compounds **36**, **43**,

Table 1
Structure and biological activity of cHTC derivatives **14–22** modified at the C-3 position.

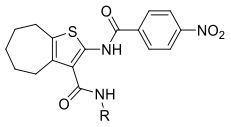

Compd	R	ELISA PA-PB1 Interaction Assay IC_{50}, μM[a]	PRA in MDCK cells EC_{50}, μM[b]	Cytotoxicity (MTT Assay) in MDCK cells CC_{50}, μM[c]	SI[d]
13		6.0 ± 1.0	0.23 ± 0.01	>250	>1087
14		125 ± 42	0.19 ± 0.01	>250	>1316
15	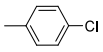	>200	1.3 ± 0.6	>250	>192
16	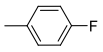	>200	81 ± 3	>250	>3
17	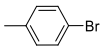	>200	3.2 ± 1.2	>250	>78
18	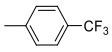	>200	0.66 ± 0.8	>250	>250
19	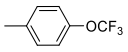	>200	4.6 ± 2.8	>250	>54
20	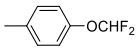	>200	2.7 ± 1.3	>250	>93
21	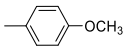	>200	>100	>250	–
22		>200	0.38 ± 0.11	73 ± 38	192
$PB1_{1-15}$-Tat peptide		35 ± 4	41 ± 5	>100	>2
RBV		–	8.7 ± 0.8	>250	>29
FPV		–	7.7 ± 0.4	>250	>32

[a] Activity of the compounds in ELISA PA-PB1 interaction assays. The IC_{50} value represents the compound concentration that reduces by 50 % the interaction between PA and PB1.
[b] Activity of the compounds in plaque reduction assays with the IAV/PR/8/34 strain. The EC_{50} value represents the compound concentration that inhibits 50 % of plaque formation.
[c] Cytotoxicity of the compounds in MTT assays. The CC_{50} value represents the compound concentration that causes a 50 % decrease in cell viability. All the reported values represent the means ± SD of data derived from at least three independent experiments in duplicate.
[d] SI: selectivity index (SI=CC_{50}/EC_{50}). RBV: ribavirin; FPV: favipiravir.

and **45** were also evaluated for cytotoxicity in HEK 293T cells by MTT assays, to exclude that the observed inhibition might be due to toxic effects of the compounds.

As expected, compounds **43** and **45** exhibited a potent inhibitory effect on IAV RdRP activity, with EC_{50} values of 0.032 and 0.13 μM, respectively (Table 4), suggesting that disruption of PA-PB1 heterodimerization resulted in potent inhibition of IAV RdRP functions. In contrast, compound **36**, which did not inhibit PA-PB1 interaction, neither inhibited RdRP activity. Notably, in contrast to the inhibitory activity of PA-PB1 determined by ELISA, the inhibitory activity of RdRP correlates with the anti-IV activity of compounds **43** and **45**, suggesting that inhibition of RdRP underlies their antiviral activity.

2.5. Compounds *43* and *45* bound the PA_C terminal domain

To determine whether the best compounds **43** and **45** interfere with PA-PB1 heterodimerization by binding to PA_C (aa 239–716), we performed biophysical experiments using nano-differential scanning fluorimetry (nano-DSF) [48]. The $PB1_N$ (aa 1–15) peptide and compound **36** were included as positive and negative controls for PA binding, respectively.

As reported in Fig. S1 and Table S1, in the nano-DSF assay, compounds **43** and **45** were able to induce a significant melting temperature shift (ΔTm) compatible with a binding to PA_C and in keeping with the results obtained in the ELISA, while compound **36** did not significantly alter the Tm. These results are consistent with those observed in the PA-PB1 interaction inhibition assay and the IV RdRP inhibition assay (minireplicon). At this point, in order to confirm the results obtained for compound **45** regarding the binding to PA_C, we evaluated its affinity to PA_C (aa 239–716) at different concentrations by the MicroScale Thermophoresis (MST) binding assay [49] as a biophysical experiment orthogonal to nanoDSF, including the $PB1_N$ (aa 1–15) peptide as a positive control.

Extrapolation of the binding curve showed a K_d value of 5.75 ± 1.27

Table 2
Structure and biological activity of cHTC derivatives **23–32** modified at the C-2 position.

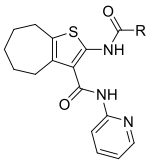

Compd	R	ELISA PA-PB1 Interaction Assay IC_{50}, μM[a]	PRA in MDCK cells EC_{50}, μM[b]	Cytotoxicity (MTT Assay) in MDCK cells CC_{50}, μM[c]	SI[d]
23	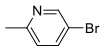	143 ± 25	>100	>250	–
24	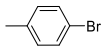	78 ± 23	>100	>250	–
25	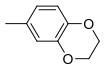	>200	>100	>250	–
26		93 ± 8	22 ± 6	28 ± 5	–
27		>200	1.0 ± 0.2	>250	>250
28		>200	97 ± 4	>250	–
29	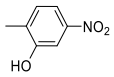	80 ± 11	1.3 ± 0.4	188 ± 8	144
30	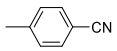	103 ± 60	1.6 ± 0.4	141 ± 25	88
31	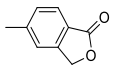	143 ± 26	17.8 ± 2.5	>100	>6
32	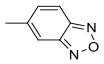	75 ± 18	>10.5	10.5 ± 0.7	–

[a-d] For the definition of IC_{50}, EC_{50}, CC_{50}, and SI, see Table 1 caption.

μM and 30.49 ± 18.55 μM for compound **45** and for $PB1_N$, respectively, supporting the data obtained by nanoDSF (Fig. S2).

In conclusion, these data demonstrated that compounds **43** and **45** inhibit IV replication and RdRP activity by disrupting PA-PB1 interaction through the binding to PA_C.

Further studies are needed to determine the binding mode of cHTC compounds to the PA_C terminal domain. In this regard, the generation of escape mutants is a valid technique for the enforcement of data about the mechanism of action of antiviral agents, although the rapid emergence of resistant variants may represent a weakness of future drugs. As mentioned above, one of the main advantages of targeting the PA-PB1 interaction is the high barrier to resistance, as the IV should simultaneously mutate both surfaces involved in the interaction between PA and PB1 to develop resistance while maintaining the subunit interaction. Consistent with this, we were not able to isolate viruses resistant to hit compound **13** (Fig. 2) [41] and the benzoimidazol-2-one compound **4** (Fig. 1) [35], highlighting a high barrier to drug resistance of PA-PB1 inhibitors. This behavior precludes on the other hand the possibility of identifying amino acids involved in their binding to PA_C.

Alternatively, we are currently attempting co-crystallization of compound **45** with PA_C. In this regard, it is worth noting that obtaining the three-dimensional structure of PA_C in complex with small molecules still represents a significant challenge, as evidenced by the lack of such structures in the literature.

*2.6. Compounds **43** and **45** showed potent, broad-spectrum, and specific anti-IV activity*

Based on the ability to interfere with PA-PB1 heterodimerization and the potent anti-IAV activity shown by compounds **43** and **45**, in depth studies were performed to further investigate their antiviral activity.

Initially, the spectrum of anti-IV activity was determined. Compounds **43** and **45** were tested by PRA against two IAV strains belonging to different co-circulating subtypes, *i.e.*, H1N1 A/Parma/24/09 oseltamivir-resistant strain and H3N2 A/Wisconsin/67/05 strain, and two IBV strains corresponding to the two distinct lineages, *i.e.*, B/Lee/40 (ancestral) and B(128)B/Malaysia/2506/04 (Victoria) (Table 5). RBV was included as a positive control. Results showed that both compounds inhibited the tested IAV and IBV strains with potency comparable to that against IAV/PR/8/34 (H1N1). In particular, compound **43** showed EC_{50} values ranging from 0.22 to 0.38 μM, while compound **45** exhibited EC_{50} values within the nanomolar range, from 54 to 89 nM. These data demonstrated that compounds **43** and **45** are potent and broad-spectrum anti-IV compounds, able to provide cross-protection against circulating subtypes of human IAV and two different lineages of IBV.

To further investigate the therapeutic potential and specificity of compounds **43** and **45**, their antiviral activity was evaluated against another negative-stranded respiratory RNA virus (human parainfluenza virus, HPIV), a positive-stranded respiratory RNA virus (SARS-CoV-2),

Table 3
Structure and biological activity of cHTC derivatives **33–46** modified at the C-2 and C-3 positions.

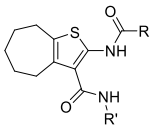

Compd	R'	R	ELISA PA-PB1 Interaction Assay IC_{50}, μM[a]	PRA in MDCK cells EC_{50}, μM[b]	Cytotoxicity (MTT Assay) in MDCK cells CC_{50}, μM[c]	SI[d]
33	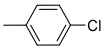	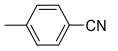	145 ± 28	0.68 ± 0.11	>250	>368
34	“	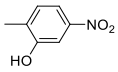	17.3 ± 4.9	N.D.[e]	115 ± 22	–
35	“		>200	62 ± 8	>250	>4
36	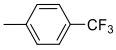	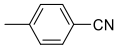	>200	1.8 ± 1.1	>250	>135
37	“		>200	0.44 ± 0.07	>200	>455
38	“	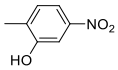	>200	N.D.[e]	10.0 ± 5.7	–
39	“		112 ± 18	1.3 ± 0.5	>100	>74
40		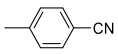	62.5 ± 17.7	N.D.[e]	>250	–
41	“	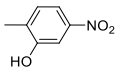	36.0 ± 8.5	N.D.[e]	64.5 ± 19.1	–
42	“		>200	0.085 ± 0.01	>250	>2941
43		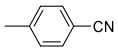	19.3 ± 6.7	0.38 ± 0.12	>250	>667
44	“		>200	0.74 ± 0.06	106 ± 6	143
45	“	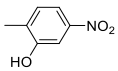	26.5 ± 4.9	0.089 ± 0.02	224 ± 23	2517
46	“		>200	0.73 ± 0.39	57.7 ± 16.3	79

[a-d] For the definition of IC_{50}, EC_{50}, CC_{50}, and SI, see Table 1 caption.
[e] N.D., not determined.

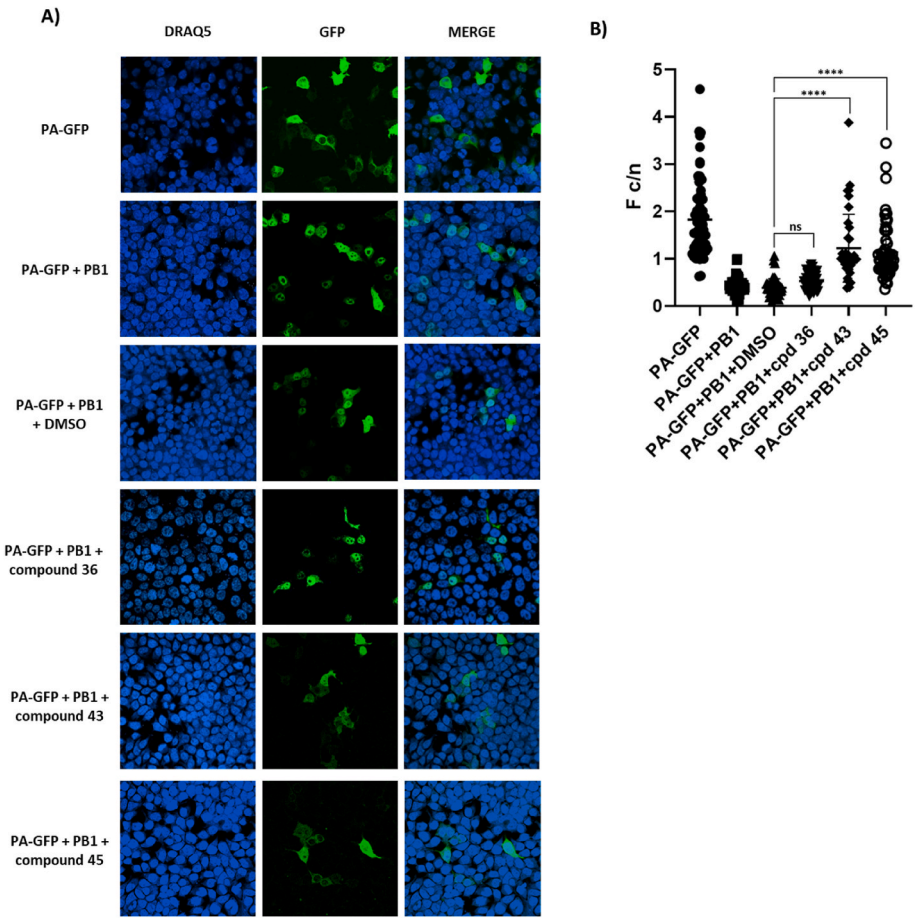

Fig. 4. Effects of compounds **36**, **43**, and **45** on intracellular localization of the PA-PB1 complex. **A.** HEK 293T cells were transfected with plasmids expressing PB1 and a PA-GFP fusion protein in the absence or the presence of test compounds or DMSO as a control. Cells transfected with the PA-GFP-expressing plasmid alone served as a negative control. At 14 h post-transfection, cells were examined by confocal laser scanning microscopy. Individual green (GFP) and blue (DRAQ5) channels and merged images are shown. **B.** Quantitative analysis of PA-GFP intracellular localization. The cytoplasmic/nuclear fluorescence ratio (Fc/n) was calculated for each tested condition. Data are presented as scatter-dot-plots of $n \geq 50$ analyzed fields from two independent experiments. Data were analyzed by one-way Anova followed by Dunnett's multiple-comparisons test. ****: $p < 0.0001$ compared to control (DMSO-treated cells).

Table 4
Activity of compounds **36**, **43**, and **45** against viral polymerase.

Compd	Minireplicon Assay EC_{50}, μM[a]	Cytotoxicity (MTT Assay) in HEK 293T cells CC_{50}, μM[b]
36	>10	>50
43	0.032 ± 0.010	>50
45	0.13 ± 0.03	>50
RBV	21.7 ± 7.3	>50
FPV	10.7 ± 2.8	>50

[a] The EC_{50} value represents the compound concentration that reduces by 50 % the activity of IAV virus RNA polymerase in HEK 293T cells.
[b] Cytotoxicity of the compounds in MTT assays. The CC_{50} value represents the compound concentration that causes a 50 % decrease in cell viability. All data shown represent the means ± SD of data derived from at least two independent experiments in duplicate. RBV: ribavirin; FPV: favipiravir.

and finally other positive-stranded RNA viruses (*i.e.,* Dengue virus, DENV, and West Nile virus, WNV). In parallel, the cytotoxicity was determined in the same cell lines used for the antiviral assays (*i.e.,* Huh7 for DENV and WNV, Caco-2 for SARS-CoV-2, and A549 for HPIV). Compounds **43** and **45** did not inhibit the replication of any of the tested viruses while being non-toxic, with the exception of compound **45**, which showed a weak anti-HPIV activity with an EC_{50} of 21.7 μM (CC_{50} > 40 μM) (data not shown). These data demonstrated a specific antiviral activity toward IAV and IBV for compounds **43** and **45**, according to their peculiar mechanism of action involving the PA-PB1 interaction disruption.

Table 5
Activity of compounds **43** and **45** against a panel of IAV and IBV strains.

Influenza Virus (strain)	PRA (EC_{50}, μM)[a]		
	43	**45**	**RBV**
A/PR/8/34 (H1N1)	0.38 ± 0.12	0.089 ± 0.016	7.4 ± 0.7
A/Parma/24/09 (H1N1) (oseltamivir-resistant)	0.28 ± 0.11	0.081 ± 0.011	22.0 ± 1.4
A/Wisconsin/67/05 (H3N2)	0.22 ± 0.06	0.054 ± 0.015	5.8 ± 1.1
B/Lee/40 (ancestral)	0.30 ± 0.03	0.087 ± 0.012	19.5 ± 3.5
B/Malaysia/2506/04	0.35 ± 0.06	0.088 ± 0.011	10.8 ± 2.5

[a] The EC_{50} value represents the compound concentration that inhibits 50 % of plaque formation. All data shown represent the means ± SD of data derived from at least two independent experiments. RBV: ribavirin.

*2.7. Compounds **43** and **45** caused a dose-dependent reduction of infectious viral progeny in human lung cells*

To further characterize the anti-IV activity of compounds **43** and **45**, we assessed their effects on the production of infectious progeny in a multi-cycle growth assay in human lung cells, along with FPV, used as a positive control. As reported in Fig. 5, for both **43** and **45** we observed a

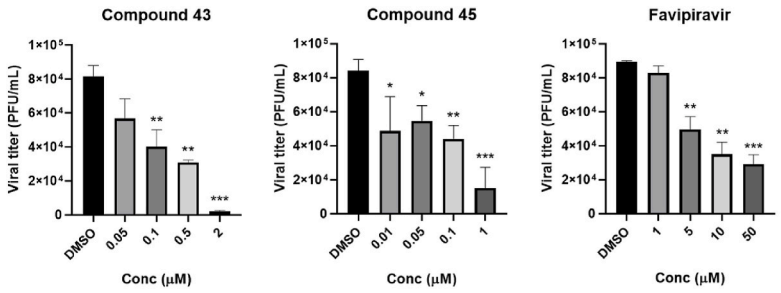

Compound	EC_{50} (μM)
43	0.14 ± 0.03
45	0.087 ± 0.021
FPV	7.93 ± 0.72

Fig. 5. Antiviral activity of compounds **43** and **45** in infected human A549 cells was determined by virus yield reduction assays. A549 cells were infected with IAV PR/8 at MOI = 0.01 and treated with different concentrations of compounds **43, 45**, FPV, or DMSO as a control. At 24 h p.i., virus progeny titers produced in the presence of test compounds were determined by titration onto fresh MDCK cell monolayers by plaque assays. Data shown are the means ± SD of three experiments performed in duplicate. Data were analyzed by a one-way ANOVA followed by Dunnett's multiple-comparisons test. ***p < 0.001; **p < 0.01; *p < 0.05 *versus* IAV-infected, DMSO-treated cells. EC_{50} values were obtained by the nonlinear regression analysis using GraphPad Prism version 10.0. FPV: favipiravir.

significant dose-dependent reduction in the production of infectious viral progeny in infected human lung A549 cells. Of note, the EC_{50} values were consistent with those observed in PRA, as compound **43** showed an EC_{50} of 0.14 μM, while the most potent compound **45** exhibited an EC_{50} of 87 nM.

2.8. Compound *45* showed a good ADME profile

To further characterize the potent compounds **43** and **45**, some pharmacokinetic properties were experimentally determined, *i.e.*, solubility (thermodynamic solubility in aqueous media), permeability [by parallel artificial membrane permeation assay (PAMPA)], and metabolic stability in human liver microsomes (HLM) and plasma.

Thermodynamic solubility in aqueous media was determined for compounds **43**, **45**, and starting hit compound **13** (Table 6). Compound **13** exhibited a suboptimal aqueous solubility of 1.72 μM (0.75 μg/mL) with a logarithm of Solubility (LogS) value of −5.76. An increased water solubility was shown by compound **43** and, even more, compound **45**, exhibiting values of 17.6 μM (7.62 μg/mL) and 49.8 μM (23.30 μg/mL), respectively (LogS = −4.75 and −4.30). These results were in accordance with permeability studies (Table 6), which underlined how the major hydrophilicity of compound **45** was responsible for a minor tendency of this derivative to cross the phospholipidic bilayer (Papp = 0.78 cm/sec x 10^{-6}) and interact with the lipid membrane (MR = 2.50 %). Compound **43**, instead, endowed with a lower water solubility, showed a higher tendency to cross membrane (Papp = 3.48 cm/sec x 10^{-6}) and interact with lipid bilayer, where probably it remained entrapped (MR = 57 %).

Then, the metabolic stability of compounds **43** and **45** in HLM was evaluated including furosemide as reference compound. Both the compounds showed high stability when incubated for 1 h in presence of HLM (Fig. 6A and Table S2), with percentages of the unmetabolized compound of 93.34 % and 93.77 %, respectively. Compounds underwent oxidative reactions that led to the introduction of one or two hydroxyl groups in different positions of the aromatic rings.

Finally, the stability of compounds **43** and **45** in the presence of plasma was assessed including dasatinib as reference compound. Compounds were incubated at a fixed concentration with plasma for different time points (from time 0 to 1440 min). While the stability of compound **45** (about 100 % throughout the experiment) resulted not to be affected by the hydrolytic action of plasma esterase, compound **43** showed decreasing plasma stability over the different time points (Fig. 6B and Table S3). Just after 5 min of incubation with plasma, the percentage of the unmodified compound began to reduce to 95 %, remaining stable until 60 min of treatment, and finally fell down to around 81 % after 1440 min.

Table 6
Equilibrium solubility and PAMPA.

Compd	**43**	**45**	**13**
Solubility[a]	17.6 μM 7.62 μg/mL	49.8 μM 23.30 μg/mL	1.72 μM 0.75 μg/mL
LogS[b]	−4.75	−4.30	−5.76
Papp[c] **cm/sec x 10^{-6}**	3.48	0.78	N.D.
% MR[d]	57	2.50	N.D.

[a] Equilibrium solubility in water.
[b] Logarithm of Solubility.
[c] Apparent permeability.
[d] Membrane retention %.

3. Conclusions

In this study, extensive medicinal chemistry efforts starting from the cHTC derivative **13** led to obtain compound **45**, which represents the most potent anti-IV compound acting by inhibiting PA-PB1 interaction identified to date, with an improved profile in terms of PK properties. Compound **45** exhibited an impressive EC_{50} value of 89 nM against IAV strain (A/PR/8/34 - H1N1) coupled with a CC_{50} value of 224 μM in MDCK cells, resulting in a very high SI (SI = 2517), and an innovative mechanism of action. Comparable potency was also demonstrated against a panel of circulating human IAV and IBV strains, highlighting its broad spectrum of activity.

In terms of characterizing the mechanism of action, compound **45** demonstrated a significant ability to disrupt the interaction between PA and PB1 both *in vitro* in the ELISA and in the cellular context, resulting in a reduction in the nuclear localization of PA in compound-treated cells. Additionally, for the first time, we focused efforts on the evaluation of the binding of cHTC compounds to PA_C using two biophysical orthogonal techniques (*i.e.,* nano-DSF and MST). Compound **45** showed a K_d of 5.75 μM, further proving that its anti-IV is strongly dependent on the disruption of the PA-PB1 interaction through the binding to PA_C. Finally, it is worth noting that the disruption of PA-PB1 interaction exerted by compound **45** resulted in the inhibition of IAV RdRP assembly and activity in the cellular context, as demonstrated by the translocation and minireplicon assays, respectively, and in the reduction of the production of infectious progeny in human disease-relevant cells. In accordance with this peculiar mechanism of action, the most potent compound **45** was not able to inhibit the viral growth of diverse RNA viruses (HPIV, SARS-CoV-2, DENV, and WNV).

Although the starting hit **13** also exhibited this specific mechanism of action, the main advancement achieved with this study relies in the fact that we succeeded in the optimization and synthesis of the new compound **45** that retains the ability to inhibit PA-PB1 interaction despite the presence of two polar groups in its chemical structure. This result is significant from a medicinal chemistry point of view due to the hydrophobic and challenging nature of the target PA_C cavity, which binds $PB1_N$ mainly through hydrophobic interactions, thus complicating the development of PPI inhibitors with drug-like properties. Therefore, the

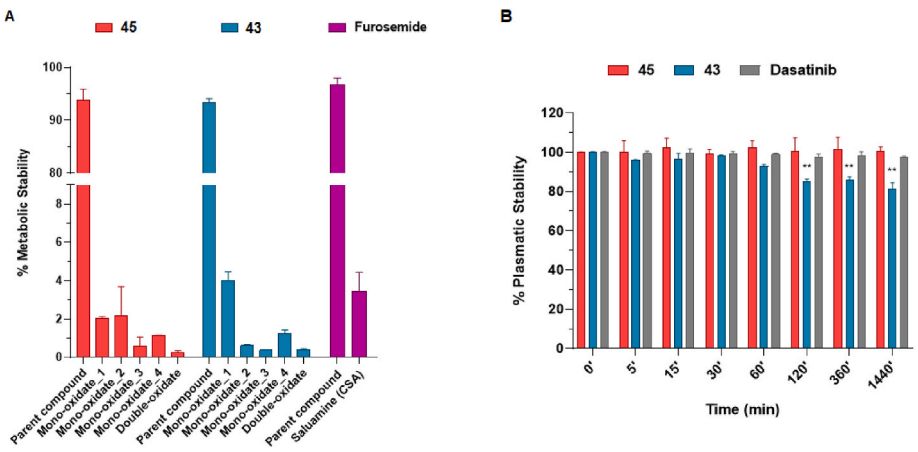

Fig. 6. A) Metabolic stability in HLM and **B)** Plasma stability of compounds **43**, **45**, and the reference compounds furosemide and dasatinib.

presence of polar groups in compound **45** made it significantly more soluble than the starting hit **13** (49.8 μM *vs* 1.72 μM), without compromising metabolic and plasma stabilities. Although the increased water solubility of compound **45** is still suboptimal for its *in vivo* evaluation, this study represents a significant step forward in the design of more polar PA-PB1 disruptors with potential *in vivo* efficacy, which has not yet been demonstrated.

4. Experimental section

4.1. Chemistry

Commercially available starting materials, reagents, and solvents were used as supplied. Compounds **47** [42], **48** [40], **49** [40], **50** [40], **57** [40], **58** [40], **59** [40], **61** [43], **64** [44], **65** [44], **67** [42], and **68** [39] were synthesized as reported in literature. Target compound **26** was synthesized as previously reported by us [50]. All reactions were routinely monitored by TLC on silica gel 60F254 (Merck) and visualized by using UV or iodine. Flash column chromatography was performed on Merck silica gel 60 (mesh 230–400). After extraction, organic solutions were dried over anhydrous Na_2SO_4, filtered, and concentrated with a Büchi rotary evaporator at reduced pressure. Yields are of purified product and were not optimized. ^{1}H NMR and ^{13}C NMR spectra were recorded on Bruker Avance DRX-400. Chemical shifts (δ) are reported in ppm relative to TMS and calibrated using residual undeuterated solvent as internal reference. Coupling constants (J) are reported in Hz. Spectra were acquired at 298 K. Data processing were performed with Bruker TopSpin 4.2.0 software, and the spectral data are consistent with the assigned structures. The spin multiplicities are indicated by the symbols: s (singlet), d (doublet), t (triplet), q (quartet), m (multiplet), and bs (broad singlet). For compounds **14**, **15** and **31–46**, the purity (>95 %) was revealed at 254 nm and evaluated by HPLC analysis using a Jasco LC-4000 instrument equipped with a UV–Visible Diode Array Jasco MD-4015 and an XTerra MS C18 Column, 5 μm, 4.6 mm × 150 mm or a Gemini LC C18 110 Å column, 3 μm, 100 mm × 2 mm (for compound **14**). Used methods have been specified for each compound. Chromatograms were analyzed by ChromNAV 2.0 Chromatography Data System software. For compounds **16–25** and **27–30**, the purity (>95 %) was evaluated by HPLC analysis using an Agilent 1290 Infinity System machine equipped with DAD detector from 190 to 640 nm. The purity was revealed at 254 nm using a Phenomenex AERIS Widepore C4, 4.6 mm, 100 mm (6.6 lm) with flow rate: 0.85 mL/min; acquisition time: 10 min; gradient: acetonitrile in water containing 0.1 % of formic acid (0–100 % in 10 min); oven temperature, 30 °C. Peak retention time is given in minutes. HRMS detection was based on electrospray ionization (ESI) in positive or negative polarity, as indicated for each compound, using Agilent 1290 Infinity System equipped with a MS detector Agilent 6540UHD Accurate Mass Q-TOF.

4.2. General procedure for the preparation of 2-cyano-N-(substituted) acetamide derivatives (method A)

To a solution of the appropriate amine (1.0 equiv) in toluene, compound **47** [42] (1.0 equiv) was added. The mixture was refluxed for 1 h and then stirred at rt to obtain a precipitate which was filtered, washed with Et_2O and dried.

4.2.1. N-(4-Bromophenyl)-2-cyanoacetamide (51)

The title compound was prepared through Method A by using 4-bromoaniline, in 78 % yield as white solid.^{1}H NMR (400 MHz, DMSO-d_6): δ 3.88 (s, 2H, CH_2), 7.47–7.56 (m, 4H, aromatic CH), 10.40 (s, 1H, NH).

4.2.2. 2-Cyano-N-[4-(trifluoromethyl)phenyl]acetamide (52)

The title compound was prepared through Method A by using 4-(trifluoromethyl)aniline, in 73 % yield as white solid. ^{1}H NMR (400 MHz, DMSO-d_6): δ 4.00 (s, 2H, CH_2), 7.67 and 7.72 (d, J = 8.7 Hz, each 2H, aromatic CH), 10.73 (s, 1H, NH).

4.2.3. 2-Cyano-N-[4-(trifluoromethoxy)phenyl]acetamide (53)

The title compound was prepared through Method A by using 4-(trifluoromethoxy)aniline, in 67 % yield as a white solid. ^{1}H NMR (400 MHz, DMSO-d_6): δ 3.96 (s, 2H, CH_2), 7.31 and 7.61 (d, J = 9.0 Hz, each 2H, aromatic CH), 10.62 (s, 1H, NH).

4.2.4. 2-Cyano-N-[4-(difluoromethoxy)phenyl]acetamide (54)

The title compound was prepared through Method A by using 4-(difluoromethoxy)aniline, in 81 % yield as a white solid. ^{1}H NMR (400 MHz, DMSO-d_6): δ 3.76 (s, 2H, CH_2), 7.12 (t, J_{HF} = 74 Hz, 1H, CHF_2), 7.12 and 7.54 (d, J = 8.9 Hz, each 2H, aromatic CH), 10.43 (s, 1H, NH).

4.2.5. N-(4-Methoxyphenyl)-2-cyanoacetamide (55)

The title compound was prepared through Method A by using 4-methoxyaniline, in 89 % yield as white solid. ^{1}H NMR (400 MHz, DMSO-d_6): δ 3.57 (s, 3H, CH_3), 3.68 (s, 2H, CH_2), 6.86 and 7.41 (d, J = 12.3 Hz, each 2H, aromatic CH), 10.22 (s, 1H, NH).

4.2.6. 2-Cyano-N-(2-methoxyphenyl)acetamide (56)

The title compound was prepared through Method A by using 2-methoxyaniline, in 50 % yield as white solid. ^{1}H NMR (200 MHz, DMSO-d_6): δ 3.52 (s, 2H, CH_2), 3.87 (s, 3H, CH_3), 6.91 (m, 2H, aromatic CH), 7.08 (m, 1H, aromatic CH), 8 8.21 (dd, J = 1.63 Hz and 7.9 Hz, 1H, aromatic CH), 8.29 (bs, 1H, NH).

4.3. General procedure for the preparation of 2-amino-N-(substituted)-cycloheptathiophene-3-carboxamides (method B)

A mixture of the appropriate 2-cyano-*N*-(substituted)acetamide (1.0 equiv), cycloheptanone (4.0 equiv), ammonium acetate (1.3 equiv), and glacial acetic acid (3.5 equiv) in dry benzene (10 mL/mmol) was heated at reflux for 16 h in a Dean-Stark apparatus. After cooling, the mixture was diluted with $CHCl_3$ and then washed with H_2O, 10 % Na_2CO_3 solution, and finally H_2O. The organic layer was concentrated to dryness to afford the crude Knoevenagel product, which was used in the successive step without further purification. Thus, to the crude Knoevenagel product (1.0 equiv) dissolved in EtOH dry, sulfur (4.0 equiv) and *N,N*-diethyl amine (4.0 equiv) were added. The mixture was maintained at 50 °C for 2 h and then concentrated to dryness to yield a residue, which was treated with Et_2O and filtered.

4.3.1. 2-Amino-N-(4-bromophenyl)-5,6,7,8-tetrahydro-4H-cyclohepta[b]thiophene-3-carboxamide (60)

The title compound was prepared starting from **51** through Method B, in 94 % yield as white-pink solid. ^{1}H NMR (400 MHz, DMSO-d_6): δ 1.40–1.60 (m, 4H, cycloheptane CH_2), 1.65–1.80, 2.40–2.55 and 2.60–2.70 (m, each 2H, cycloheptane CH_2), 5.80 (bs, 2H, NH_2), 6.75 and 7.25 (d, J = 8.0 Hz, each 2H, aromatic CH), 9.50 (s, 1H, NH).

4.3.2. 2-Amino-N-[4-(trifluoromethoxy)phenyl]-5,6,7,8-tetrahydro-4H-cyclohepta[b]thiophene-3-carboxamide (62)

The title compound was prepared starting from **53** through Method B, in 100 % yield as brown solid. ^{1}H NMR (400 MHz, DMSO-d_6): δ 1.50–1.54 (m, 4H, cycloheptane CH_2), 1.63–1.73, 2.51–2.55 and 2.60–2.62 (m, each 2H, cycloheptane CH_2), 5.98 (bs, 2H, NH_2), 7.27 and 7.73 (d, J = 8.7 Hz, each 2H, aromatic CH), 9.95 (s, 1H, NH).

4.3.3. 2-Amino-N-[4-(difluoromethoxy)phenyl]-5,6,7,8-tetrahydro-4H-cyclohepta[b]thiophene-3-carboxamide (63)

The title compound was prepared starting from **54** through Method B, in 95 % yield as brown solid. ^{1}H NMR (400 MHz, DMSO-d_6): δ 1.44–1.53 (m, 4H, cycloheptane CH_2), 1.65–1.72 (m, 2H, cycloheptane CH_2), 2.50–2.57 (m, 2H, cycloheptane CH_2), 2.60–2.62 (m, 2H, cycloheptane CH_2), 5.88 (bs, 2H, NH_2), 7.10 (t, J_{HF} = 62.5 Hz, 1H, CHF_2), 7.07 and 7.65 (d, J = 9.0 Hz, each 2H, aromatic CH), 9.56 (s, 1H, NH).

4.4. General procedure for C-2 amidation (method C)

A solution of the appropriate intermediate (1.0 equiv) in dry pyridine was added to the suitable benzoyl chloride (2.0 equiv). The reaction mixture was maintained at rt until no starting material was detected by TLC. Then, the reaction mixture was poured into ice/water, obtaining a precipitate that was filtered and purified as described below.

4.4.1. 2-[(4-Nitrobenzoyl)amino]-N-1,3-thiazol-2-yl-5,6,7,8-tetrahydro-4H-cyclohepta[b]thiophene-3-carboxamide (14)

The title compound was prepared starting from **57** [40] through Method C using 4-nitrobenzoyl chloride and purified by flash chromatography eluting with cyclohexane/EtOAc (80:20) followed by crystallization in EtOH, in 10 % yield as orange solid. ^{1}H NMR (400 MHz, DMSO-d_6): δ 1.43–1.51 (m, 4H, cycloheptane CH_2), 1.68–1.78 (m, 2H, cycloheptane CH_2), 2.62–2.72 (m, 4H, cycloheptane CH_2), 7.18 and 7.49 (d, J = 4.0 Hz, each 1H, thiazole CH), 8.09 and 8.31 (d, J = 8.3 Hz, each 2H, aromatic CH), 11.50 and 12.34 (s, each 1H, NH). ^{13}C NMR (101 MHz, DMSO-d_6): δ 27.61, 28.01, 28.24. 28.89, 32.42, 113.53, 124.14, 129.76, 130.40, 131.30, 137.15, 139.44, 149.74, 141.10, 150.60, 154.53, 159.29, 162.89. HRMS (ESI) m/z [M − H]$^-$ calcd for $C_{20}H_{18}N_4O_4S_2$ 442.07695, found 442.0767. HPLC, RP C18 (Gemini - Phenomenex), H_2O with 0.1 % FA 20 %/CH_3CN 80 % to CH_3CN 100 % in 10 min, ret. time: 9.710 min.

4.4.2. N-(4-Chlorophenyl)-2-[(4-nitrobenzoyl)amino]-5,6,7,8-tetrahydro-4H-cyclohepta[b]thiophene-3-carboxamide (15)

The title compound was prepared starting from **58** [40] through Method C using 4-nitrobenzoyl chloride and purified by flash chromatography eluting with CH_2Cl_2 (100), in 19 % yield as yellow solid. ^{1}H NMR (400 MHz, DMSO-d_6): δ 1.57–1.66 (m, 4H, cycloheptane CH_2), 1.81–1.89 (m, 2H, cycloheptane CH_2), 2.69–2.81 (m, 4H, cycloheptane CH_2), 7.38 (d, J = 7.7 Hz, 2H, aromatic CH), 7.77 (d, J = 7.0 Hz, 2H, aromatic CH), 8.13 (d, J = 7.5 Hz, 2H, aromatic CH), 8.34 (d, J = 7.3 Hz, 2H, aromatic CH), 10.27 and 11.24 (s, each 1H, NH). ^{13}C NMR (101 MHz, DMSO-d_6): δ 27.77, 28.39, 28.47, 29.06, 32.35, 121.87, 124.19, 126.14, 127.55, 129.03, 129.77, 132.94, 134.55, 136.56, 138.91, 139.49, 149.93, 163.16, 163.66. HRMS (ESI) m/z [M − H]$^-$ calcd for $C_{23}H_{20}ClN_3O_4S$ 468.0790, found 468.0779. HPLC, H_2O 20 %/CH_3CN 80 %, ret. time: 4.3967 min.

4.4.3. N-(4-Fluorophenyl)-2-[(4-nitrobenzoyl)amino]-5,6,7,8-tetrahydro-4H-cyclohepta[b]thiophene-3-carboxamide (16)

The title compound was prepared starting from **59** [40] through Method C using 4-nitrobenzoyl chloride and purified by flash chromatography eluting with cyclohexane/EtOAc (80:20), in 20 % yield as yellow solid. ^{1}H NMR (400 MHz, DMSO-d_6): δ 1.37–1.57 (m, 4H, cycloheptane CH_2), 1.76–1,78 (m, 2H, cycloheptane CH_2), 2.62–2.70 (m, 4H, cycloheptane CH_2), 7.13 and 7.74 (m, each 2H, aromatic CH), 8.02 and 8.30 (d, J = 8.52 Hz, each 2H, aromatic CH), 10.25 and 11.29 (s, each 1H, NH). ^{13}C NMR (101 MHz, DMSO-d_6): δ 27.70, 28.31, 28.94, 31.57, 32.33, 115.60 (d, J_{CF} = 22 Hz), 121.88, 124.11, 125.99, 129.68, 132.72, 134.17, 136.24, 136.48, 139.34, 149.74, 162.98, 158.37 (d, J_{CF} = 220 Hz), 163.31. HRMS (ESI) m/z [M − H]$^-$ calcd for $C_{23}H_{20}FN_3O_4S$ 453.11586, found 453.11554. HPLC, ret. time: 6.613 min.

4.4.4. N-(4-Bromophenyl)-2-[(4-nitrobenzoyl)amino]-5,6,7,8-tetrahydro-4H-cyclohepta[b]thiophene-3-carboxamide (17)

The title compound was prepared starting from **60** through Method C using 4-nitrobenzoyl chloride and purified by crystallization by Et_2O/EtOH, in yield 12 %, as yellow solid. ^{1}H NMR (400 MHz, DMSO-d_6): δ 1.50–1.60 (m, 4H, cycloheptane CH_2), 1.72–1.78 (m, 2H, cycloheptane CH_2), 2.26–2.70 (m, 4H, cycloheptane CH_2), 7.48, 7.70, 8.01 and 8.30 (d, J = 8.7 Hz, each 2H, aromatic CH), 10.35 and 11.30 (s, each 1H, NH). ^{13}C NMR (101 MHz, DMSO-d_6): δ 27.70, 28.30 (2C), 28.95, 32.32, 115.42, 122.10, 124.11, 125.98, 129.70, 131.86, 132.80, 133.47, 134.31, 136.50, 139.29, 147.64, 163.10, 163.50. HRMS (ESI) m/z [M − H]$^-$ calcd for $C_{23}H_{20}BrN_3O_4S$ 513.03535, found 513.03579. HPLC, ret. time: 7.020 min.

4.4.5. 2-[(4-Nitrobenzoyl)amino]-N-[4-(trifluoromethyl)phenyl]-5,6,7,8-tetrahydro-4H-cyclohepta[b]thiophene-3-carboxamide (18)

The title compound was prepared starting from **61** [43] through Method C using 4-nitrobenzoyl chloride and purified by crystallization by cyclohexane/EtOAc, in yield 32 % yield as brown solid. ^{1}H NMR (400 MHz, DMSO-d_6): δ 1.51–1.58 (m, 4H, cycloheptane CH_2), 1.75–1.82 (m, 2H, cycloheptane CH_2), 2.63–2.73 (m, 4H, cycloheptane CH_2), 7.70 and 7.93 (d, J = 8.5 Hz, each 2H, aromatic CH), 8.02 and 8.30 (d, J = 8.7 Hz, each 2H, aromatic CH), 10.82 and 11.53 (s, each 1H, NH). ^{13}C NMR (101 MHz, DMSO-d_6): δ 27.62, 28.17, 28.24, 28.86, 32.28, 119.88, 124.90 (q, J_{CF} = 228.2 Hz), 124.04, 125.68, 126.31, 126.33, 129.67, 132.80, 134.36, 136.47, 139.30, 143.48, 149.68, 163.00, 163.76. HRMS (ESI) m/z [M − H]$^-$ calcd for $C_{24}H_{20}F_3N_3O_4S$ 503.11266, found 503.11262. HPLC, ret. time: 7.060 min.

4.4.6. 2-[(4-Nitrobenzoyl)amino]-N-[4-(trifluoromethoxy)phenyl]-5,6,7,8-tetrahydro-4H-cyclohepta[b]thiophene-3-carboxamide (19)

The title compound was prepared starting from **62** through Method C using 4-nitrobenzoyl chloride and purified by crystallization in EtOH, in 33 % yield as yellow solid. ^{1}H NMR (400 MHz, DMSO-d_6): δ 1.51–1.58 (m, 4H, cycloheptane CH_2), 1.72–1.83 (m, 2H, cycloheptane CH_2),

2.63–2.74 (m, 4H, cycloheptane CH_2), 7.32 and 7.89 (d, $J = 8.6$ Hz, each 2H, aromatic CH), 8.02 and 8.30 (d, $J = 8.7$ Hz, each 2H, aromatic CH), 10.04 and 11.30 (s, each 1H, NH). ^{13}C NMR (101 MHz, DMSO-d_6): δ 27.63, 28.23 (2C), 28.86, 32.27, 121.37, 121.94, 122.83 (q, $J_{CF} = 220.0$ Hz), 124.04, 125.77, 129.65, 132.69, 134.18, 136.42, 139.08, 139.30, 144.02, 149.67, 163.00, 163.47. HRMS (ESI) *m/z* [M − H]$^-$ calcd for $C_{24}H_{20}F_3N_3O_5S$ 519.10758, found 519.10769. HPLC, ret. time: 7.111 min.

4.4.7. N-[4-(Difluoromethoxy)phenyl]-2-[(4-nitrobenzoyl)amino]-5,6,7,8-tetrahydro-4H-cyclohepta[b]thiophene-3-carboxamide (20)

The title compound was prepared starting from **63** through Method C using 4-nitrobenzoyl chloride and purified by crystallization in EtOH, in 20 % yield as orange solid. ^{1}H NMR (400 MHz, DMSO-d_6): δ 1.52–1.58 (m, 4H, cycloheptane CH_2), 1.75–1.79 (m, 2H, cycloheptane CH_2), 2.63–2.71 (m, 4H, cycloheptane CH_2), 7.12 (t, $J_{HF} = 71$ Hz, 1H, CHF_2), 7.13 and 7.76 (d, $J = 8.7$ Hz, each 2H, aromatic CH) 8.03 and 8.31 (d, $J = 8.7$ Hz, each 2H, aromatic CH), 10.34 and 11.40 (s, each 1H, NH). ^{13}C NMR (101 MHz, DMSO-d_6): δ 27.70, 28.31 (2C), 28.94, 32.34, 116.95 (t, $J_{CF} = 258.6$ Hz), 119.87, 121.48, 124.11, 125.99, 129.69, 132.74, 134.19, 136.49, 137.21, 139.33, 146.80, 149.74, 163.00, 163.38. HRMS (ESI) *m/z* [M − H]$^-$ calcd for $C_{24}H_{21}F_2N_3O_5S$ 501.1170, found 501.11703. HPLC, ret. time: 6.665 min.

4.4.8. N-(4-Methoxyphenyl)-2-[(4-nitrobenzoyl)amino]-5,6,7,8-tetrahydro-4H-cyclohepta[b]thiophene-3-carboxamide (21)

The title compound was prepared starting from **64** [44] through Method C using 4-nitrobenzoyl chloride and purified by flash chromatography eluting with cyclohexane/EtOAc (70:30), in 8 % yield, as yellow solid. ^{1}H NMR (400 MHz, DMSO-d_6) δ 1.35–1.52 (m, 4H, cycloheptane CH_2), 1.79–1.84 (m, 2H, cycloheptane CH_2), 2.63–2.72 (m, 4H, cycloheptane CH_2), 3.69 (s, 3H, OCH_3), 6.87, 7.63, 8.03 and 8.31 (d, $J = 8.8$ Hz, each 2H, aromatic CH), 10.03 and 11.28 (s, each 1H, NH). ^{13}C NMR (101 MHz, DMSO-d_6): δ 27.71, 28.28, 28.39, 28.96, 32.33, 55.63, 114.15, 121.67, 124.13, 126.18, 129.63, 132.63, 132.91, 134.11, 136.49, 139.39, 149.75, 155.83, 162.84, 163.05. HRMS (ESI) *m/z* [M − H]$^-$ calcd for $C_{24}H_{23}N_3O_5S$ 465.13562, found 465.13586. HPLC, ret. time: 6.485 min.

4.4.9. N-(2-Methoxyphenyl)-2-[(4-nitrobenzoyl)amino]-5,6,7,8-tetrahydro-4H-cyclohepta[b]thiophene-3-carboxamide (66)

The title compound was prepared starting from **65** [44] through Method C using 4-nitrobenzoyl chloride and purified by Et_2O, in 76 % yield as orange solid. ^{1}H NMR (400 MHz, DMSO-d_6): δ 1.58–1.59 (m, 4H, cycloheptane CH_2), 1.80–1.82 (m, 2H, cycloheptane CH_2), 2.72–2.74 (m, 4H, cycloheptane CH_2), 3.66 (s, 3H, CH_3), 6.92 (t, $J = 7.6$ Hz, 1H, aromatic CH), 7.01 (d, $J = 7.6$ Hz, 1H, aromatic CH), 7.07–7.11 (m, 1H, aromatic CH), 8.04–8.08 (m, 1H, aromatic CH), 8.10 and 8.34 (d, $J = 8.8$ Hz, each 2H, aromatic CH), 9.05 and 11.43 (s, each 1H, NH).

4.5. General procedure for O-demethylation (method D)

To a solution of the appropriate methoxyl derivative (1.0 equiv) in dry CH_2Cl_2, 1M solution of BBr_3 in CH_2Cl_2 (6.0 equiv) was added dropwise maintaining the temperature at 0 °C. Then, the reaction mixture was stirred at rt for 24 h and then quenched with MeOH and water. The organic solvent was removed under vacuum affording a residue, which was filtered and purified as described below.

4.5.1. N-(2-Hydroxyphenyl)-2-[(4-nitrobenzoyl)amino]-5,6,7,8-tetrahydro-4H-cyclohepta[b]thiophene-3-carboxamide (22)

The title compound was prepared starting from **66** through Method D and purified by flash chromatography eluting with cyclohexane/EtOAc (75:25), in 24 % yield as orange solid. ^{1}H NMR (400 MHz, DMSO-d_6): δ 1.52–1.59 (m, 4H, cycloheptane CH_2), 1.79–1.80 (m, 2H, cycloheptane CH_2), 2.72–2.81 (m, 4H, cycloheptane CH_2), 6.76–6.80 (m, 1H, aromatic CH), 6.83–6.86 (m, 1H, aromatic CH), 6.94–6.98 (m, 1H, aromatic CH), 7.83 (d, $J = 7.3$ Hz, 1H, aromatic CH), 8.10 and 8.33 (d, $J = 8.9$ Hz, each 2H, aromatic CH), 9.05 (s, 1H, OH), 9.92 and 11.34 (s, 1H, NH). ^{13}C NMR (101 MHz, DMSO-d_6): δ 27.46, 28.07, 28.28, 28.76, 32.14, 115.80, 119.36, 123.30, 124.23, 125.00, 125.65, 126.26, 129.53, 133.16, 135.46, 136.24, 138.83, 148.69, 149.80, 162.76, 163.44. HRMS (ESI) *m/z* [M − H]$^-$ calcd for $C_{23}H_{21}N_3O_5S$ 451.12019 found 451.11985. HPLC, ret. time: 6.337 min.

4.5.2. 5-Bromo-N-{3-[(pyridin-2-ylamino)carbonyl]-5,6,7,8-tetrahydro-4H-cyclohepta[b]thien-2-yl}pyridine-2-carboxamide (23)

The title compound was prepared starting from **68** [39] through method C using 5-bromopyridine-2-carbonyl chloride and purified by crystallization in EtOH, in 23 % yield as green solid. ^{1}H NMR (400 MHz, DMSO-d_6): δ 1.57–1.60 (m, 4H, cycloheptane CH_2), 1.70–1.72 (m, 2H, cycloheptane CH_2), 2.62–2.81 (m, 4H, cycloheptane CH_2), 7.13 and 7.82 (t, $J = 6.5$ Hz and $J = 7.2$ Hz, each 1H, pyridine CH), 8.02–8.09 (m, 2H, pyridine CH), 8.28–8.32 (m, 2H, pyridine CH), 8.88–8.93 (m, 1H, pyridine CH), 10.42 and 11.74 (s, each 1H, NH). ^{13}C NMR (101 MHz, DMSO-d_6): δ 27.39, 27.85, 28.78 (2C), 31.97, 115.06, 120.35, 122.45, 124.64, 124.80, 131.70, 135.89, 137.55, 138.56, 141.43, 146.98, 148.54, 150.30, 151.95, 160.37, 164.81. HRMS (ESI) *m/z* [M + Na]$^+$ calcd for $C_{21}H_{19}BrN_4O_2S$ 470.04121, found 470.04159 HPLC, ret. time: 6.583 min.

4.5.3. 2-[(4-Bromobenzoyl)amino]-N-pyridin-2-yl-5,6,7,8-tetrahydro-4H-cyclohepta[b]thiophene-3-carboxamide (24)

The title compound was prepared starting from **68** [39] through Method C using 4-bromobenzoyl chloride and purified by flash chromatography eluting with cyclohexane/EtOAc (90:10), in 10 % yield as white solid. ^{1}H NMR (400 MHz, DMSO-d_6): δ 1.52–1.57 (m, 4H, cycloheptane CH_2), 1.77–1.79 (m, 2H, cycloheptane CH_2), 2.71–2.74 (m, 4H, cycloheptane CH_2), 7.09 (t, $J = 6.0$ Hz, 1H, pyridine CH), 7.68 (d, $J = 7.5$ Hz, 2H, aromatic CH), 7.75–7.81 (m, 3H, aromatic CH and pyridine CH), 8.16 (d, $J = 8.3$ Hz, 1H, pyridine CH), 8.32 (d, $J = 4.53$ Hz, 1H, pyridine CH), 10.45 and 11.02 (s, each 1H, NH). ^{13}C NMR (101 MHz, DMSO-d_6): δ 27.60, 28.19, 28.33, 28.93, 32.30, 114.99, 120.07, 124.97, 126.31, 130.37, 131.99, 132.37, 132.72, 135.82, 136.51, 138.35, 148.45, 152.57, 163.70, 164.07. HRMS (ESI) *m/z* [M + H]$^+$ calcd for $C_{22}H_{20}B_rN_3O_2S$ 469.04596, found 469.04577. HPLC, ret. time: 6.847 min.

4.5.4. N-(3-(Pyridin-2-ylcarbamoyl)-5,6,7,8-tetrahydro-4H-cyclohepta[b]thiophen-2-yl)-2,3-dihydrobenzo[b][1,4]dioxine-6-carboxamide (25)

The title compound was prepared starting from **68** [39] through Method C using 2,3-dihydrobenzo[*b*][1,4]dioxine-6-carbonyl chloride and purified by flash chromatography eluting with cyclohexane/EtOAc (75:25), in 95 % yield as white solid. ^{1}H NMR (400 MHz, DMSO-d_6): δ 1.41–1.50 (m, 4H, cycloheptane CH_2), 1.58–1.61 (m, 2H, cycloheptane CH_2), 2.63–2.70 (m, 4H, cycloheptane CH_2), 4.24–4.26 (m, 4H, benzodioxane CH_2), 6.88–6.98 (m, 1H, aromatic CH), 7.08–7.10 (m, 1H, aromatic CH), 7.29–7.40 (m, 2H, aromatic CH), 7.76–7.80 (m, 1H, aromatic CH), 8.16 (d, $J = 8.2$ Hz, 1H, aromatic CH), 8.30 (s, 1H, aromatic CH), 10.32 and 10.83 (s, each 1H, NH). ^{13}C NMR (101 MHz, DMSO-d_6): δ 27.59, 28.16, 28.42, 28.90, 32.26, 64.43, 64.86, 114.99, 117.19, 117.58, 120.09, 121.64, 124.22, 126.32, 132.01, 136.33, 136.79, 138.40, 143.51, 147.29, 148.42, 152.48, 163.60, 164.33. HRMS (ESI) *m/z* [M + H]$^+$ calcd for $C_{24}H_{23}N_3O_4S$ 450.1468, found 450.1487. HPLC, ret. time: 6.230 min.

4.5.5. 2-(5-Chlorothiophene-2-carboxamido)-N-(pyridin-2-yl)-5,6,7,8-tetrahydro-4H-cyclohepta[b]thiophene-3-carboxamide (27)

The title compound was prepared starting from **68** [39] through Method C using 5-chlorothiophene-2-carbonyl chloride and purified by crystallization by EtOH, in 53 % yield as white solid. ^{1}H NMR (400 MHz, DMSO-d_6): 1.48–1.63 (m, 4H, cycloheptane CH_2), 1.73–1.82 (m, 2H,

cycloheptane CH_2), 2.62–2.79 (m, 4H, cycloheptane CH_2), 7.05–7.11 (m, 1H, pyridine CH), 7.19–7.23 (m, 1H, aromatic CH), 7.67–7.71 (m, 1H, aromatic CH), 7.78 (t, $J = 7.6$ Hz, 1H, pyridine CH), 8.18 (d, $J = 8.2$ Hz, 1H, thiophene CH), 8.27–8.31 (m, 1H, aromatic CH), 10.48 and 10.85 (s, each 1H, NH). δ ^{13}C NMR (101 MHz, DMSO-d_6): δ 27.51, 28.09, 28.24, 28.90, 32.20, 114.93, 119.99, 125.94, 128.76, 130.29, 132.91, 134.51, 134.75, 136.63, 137.38, 138.27, 148.24, 152.49, 158.18, 163.58. HRMS (ESI) *m/z* $[M + H]^+$ calcd for $C_{20}H_{18}ClN_3O_2S_2$ 432.0608, found 432.0602. HPLC, ret. time: 6.798 min.

4.5.6. N-pyridin-2-yl-2-[(3-thienylcarbonyl)amino]-5,6,7,8-tetrahydro-4H-cyclohepta[b]thiophene-3-carboxamide (28)

The title compound was prepared starting from **68** [39] through Method C using thiophene-3-carbonyl chloride and purified by flash chromatography eluting with cyclohexane/EtOAc (70:30), in 29 % yield as white solid. ^{1}H NMR (400 MHz, DMSO-d_6): δ 1.49–1.61 (m, 4H, cycloheptane CH_2), 1.75–1.83 (m, 2H, cycloheptane CH_2), 2.68–2.77 (m, 4H, cycloheptane CH_2), 7.10 (t, $J = 6.5$ Hz, 1H, aromatic CH), 7.48–7.52 (m, 1H, aromatic CH), 7.60–7.64 (m, 1H, aromatic CH), 7.77 (t, $J = 6.5$ Hz, 1H, aromatic CH), 8.18 (d, $J = 7.5$ Hz, 1H, aromatic CH), 8.23–8.26 (m, 1H, aromatic CH), 8.29–8.34 (m, 1H, aromatic CH), 10.37 and 10.76 (s, each 1H, NH). ^{13}C NMR (101 MHz, DMSO-d_6): δ 27.60, 28.17, 28.39, 28.93, 32.30, 115.02, 120.09, 124.80, 127.26, 127.88, 131.04, 132.29, 135.93, 136.46, 138.37, 148.39 (2C), 152.54, 160.09, 164.20. HRMS (ESI) *m/z* $[M + H]^+$ calcd for $C_{20}H_{19}N_3O_2S_2$ 398.0998, found 398.0991. HPLC, ret. time: 6.015 min.

4.5.7. 2-[(4-Cyanobenzoyl)amino]-N-pyridin-2-yl-5,6,7,8-tetrahydro-4H-cyclohepta[b]thiophene-3-carboxamide (30)

The title compound was prepared starting from **68** [39] through Method C using 4-cyanobenzoyl chloride and purified by crystallization in EtOH, in 13 % yield as yellow solid. ^{1}H NMR (400 MHz, DMSO-d_6): δ 1.52–1.58 (m, 4H, cycloheptane CH_2), 1.76–1.78 (m, 2H, cycloheptane CH_2), 2.68–72 (m, 4H, cycloheptane CH_2), 7.10 and 7.77 (m, each 1H, pyridine CH), 7.96 and 8.02 (d, $J = 8.4$ Hz, each 2H, aromatic CH), 8.17 (d, $J = 8.3$ Hz, 1H, pyridine CH), 8.32–8.34 (m, 1H, pyridine CH), 10.52 and 11.18 (s, each 1H, NH). ^{13}C NMR (101 MHz, DMSO-d_6): δ 27.53, 28.18 (2C), 28.87, 32.25, 114.53, 114.98, 118.62, 120.02, 125.31, 129.15, 132.59, 132.90, 135.16, 136.58, 137.64, 138.45 (2C), 152.47, 163.26, 163.85. HRMS (ESI) *m/z* $[M + H]^+$ calcd for $C_{23}H_{20}N_4O_2S$ 416.1307, found 416.13131 HPLC, ret. time: 6.052 min.

4.5.8. 1-Oxo-N-(3-(pyridin-2-ylcarbamoyl)-5,6,7,8-tetrahydro-4H-cyclohepta[b]thiophen-2-yl)-1,3-dihydroisobenzofuran-5-carboxamide (31)

The title compound was prepared starting from **68** [39] through Method C using 1-oxo-1,3-dihydroisobenzofuran-5-carbonyl chloride and purified by crystallized by EtOH/DMF, in 60 % yield as yellow solid. ^{1}H NMR (400 MHz, DMSO-d_6): δ 1.58–1.64 (m, 4H, cycloheptane CH_2), 1.80–1.86 (m, 2H, cycloheptane CH_2), 2.73–2.78 (m, 4H, cycloheptane CH_2), 5.48 (s, 2H, OCH_2), 7.15 (t, $J = 5.1$ Hz, 1H, aromatic CH), 7.82 (t, $J = 7.1$ Hz, 1H, aromatic CH), 7.97 (d, $J = 7.9$ Hz, 1H, aromatic CH), 8.07 (d, $J = 7.9$ Hz, 1H, aromatic CH), 8.17–8.22 (m, 2H, aromatic CH), 8.39 (d, $J = 3.79$ Hz, 1H, aromatic CH), 10.51 (s, 1H, CONH), 11.23 (s, 1H, CONH). ^{13}C NMR (101 MHz, DMSO-d_6): δ 27.13, 27.75, 27.85, 28.49, 31.83, 70.00, 114.57, 119.68, 122.69, 125.06, 127.65 (2C), 128.59, 132.24, 135.08, 136.20, 137.94, 138.49, 147.40, 147.98, 152.14, 163.47 (2C), 168.89. HRMS (ESI) *m/z* $[M + H]^+$ calcd for $C_{24}H_{21}N_3O_4S$ 448.1312, found 448.1345 HPLC, H_2O with 0.1 % FA 20 %/CH_3CN 80 %, ret. time: 2.7500 min.

4.5.9. N-(3-(Pyridin-2-ylcarbamoyl)-5,6,7,8-tetrahydro-4H-cyclohepta[b]thiophen-2-yl)benzo[c] [1,2,5]oxadiazole-5-carboxamide (32)

The title compound was prepared starting from **68** [39] through Method C using benzo[c][1,2,5]oxadiazole-5-carbonyl chloride and purified by crystallization by EtOH/DMF, in 60 % yield as yellow solid. ^{1}H NMR (400 MHz, DMSO-d_6): δ 1.57–1.63 (m, 4H, cycloheptane CH_2), 1.82–1.85 (m, 2H, cycloheptane CH_2), 2.75–2.79 (m, 4H, cycloheptane CH_2), 7.17 (t, $J = 5.0$ Hz, 1H, aromatic CH), 7.83 (t, $J = 7.1$ Hz, 1H, aromatic CH), 7.96 (d, $J = 9.4$ Hz, 1H, aromatic CH), 8.18 (d, $J = 9.2$ Hz, 1H, aromatic CH), 8.24 (d, $J = 8.0$ Hz, 1H, aromatic CH), 8.41 (d, $J = 4.7$, 1H aromatic CH), 8.69 (s, 1H, aromatic CH), 10.67 (s, 1H, CONH), 11.35 (s, 1H, CONH). ^{13}C NMR (101 MHz, DMSO-d_6): δ 27.16, 27.77 (2C), 28.53, 31.88, 114.98, 116.59, 117.27, 119.68, 125.43, 131.50, 132.54, 134.39, 136.40, 137.07, 137.94, 147.94, 148.67, 149.11, 152.27, 162.76, 163.14. HRMS (ESI) *m/z* $[M + H]^+$ calcd for $C_{22}H_{19}N_5O_3S$ 434.1268, found 434.1296 HPLC, H_2O with 0.1 % FA 20 %/CH_3CN 80 %, ret. time: 3.4700 min.

4.5.10. 2-[(2-Methoxy-4-nitrobenzoyl)amino]-N-pyridin-2-yl-5,6,7,8-tetrahydro-4H cyclohepta[b]thiophene-3-carboxamide (69)

The title compound was prepared starting from **68** [39] through Method C using 2-methoxy-4-nitrobenzoyl chloride and purified by treatment Et_2O, in 77 % yield as orange solid. ^{1}H NMR (400 MHz, DMSO-d_6): δ 1.56–1.60 (m, 4H, cycloheptane CH_2), 1.72–1.78 (m, 2H, cycloheptane CH_2), 2.63–2.70 (m, 2H, cycloheptane CH_2), 2.78–2.80 (m, 2H, cycloheptane CH_2), 4.05 (s, 3H, CH_3), 7.14 (dd, $J = 4.9$ Hz, and $J = 7.2$ Hz, 1H, pyridine CH), 7.80–7.86 (m, 1H, pyridine CH), 7.91–7.93 (m, 2H, aromatic CH and pyridine CH), 8.22 (t, $J = 8.7$ Hz, 1H, pyridine CH_2), 8.33 (d, $J = 5.6$ Hz, 1H, aromatic CH), 10.45 and 11.72 (s, each 1H, NH).

4.5.11. 2-[(2-Hydroxy-4-nitrobenzoyl)amino]-N-pyridin-2-yl-5,6,7,8-tetrahydro-4H-cyclohepta[b]thiophene-3-carboxamide (29)

The title compound was prepared starting from **69** through Method D and purified by flash chromatography eluting with cyclohexane/EtOAc (70:30), in 14 % yield as yellow solid. ^{1}H NMR (400 MHz, DMSO-d_6): δ 1.56–1.59 (m, 4H, cycloheptane CH_2), 1.76–1.79 (m, 2H, cycloheptane CH_2), 2.70–2.76 (m, 4H, cycloheptane CH_2), 7.11–7.13 (m, 1H, pyridine CH), 7.71–7.74 (m, 2H, aromatic CH), 7.81 (t, $J = 7.7$ Hz, 1H, pyridine CH), 8.04 and 8.17 (d, $J = 8.2$ Hz and $J = 8.6$ Hz, each 1H, pyridine CH), 8.31 (d, $J = 4.0$ Hz, 1H, aromatic CH), 10.44 and 12.06 (s, 1H, NH). ^{13}C NMR (101 MHz, DMSO-d_6): δ 27.46, 27.98, 28.72, 28.76, 32.08, 111.75, 114.36, 115.16, 120.28, 122.37, 123.23, 131.63, 133.02, 135.64, 137.03, 138.42, 148.57, 150.41, 152.02, 156.98, 160.19, 164.79. HRMS (ESI) *m/z* $[M - H]^-$ calcd for $C_{22}H_{20}N_4O_5S$ 452.11544, found 452.11541. HPLC, ret. time: 5.938 min.

4.5.12. N-(4-chlorophenyl)-2-[(4-cyanobenzoyl)amino]-5,6,7,8-tetrahydro-4H-cyclohepta[b]thiophene-3-carboxamide (33)

The title compound was prepared starting from **58** [40] through Method C using 4-cyanobenzoyl chloride and purified by crystallization by EtOH/DMF, in 41 % yield as yellow solid. ^{1}H NMR (400 MHz, DMSO-d_6): δ 1.56–1.63 (m, 4H, cycloheptane CH_2), 1.81–1.85 (m, 2H, cycloheptane CH_2), 2.71–2.79 (m, 4H, cycloheptane CH_2), 7.40 (d, $J = 8.6$ Hz, 2H, aromatic CH), 7.79 (d, $J = 8.2$ Hz, 2H, aromatic CH), 7.97–8.02 (m, 4H, aromatic CH), 10.35 and 11.26 (s, each 1H, NH). ^{13}C NMR (101 MHz, DMSO-d_6): δ 27.80, 28.40 (2C), 29.05, 32.41, 114.70, 118.75, 121.75, 125.92, 127.47, 129.04, 129.10, 132.80, 133.10, 134.54, 136.56, 137.83, 138.96, 163.37, 163.62. HRMS (ESI) *m/z* $[M + Na]^+$ calcd for $C_{24}H_{20}ClN_3O_2S$ 472.08627, found 472.08652. HPLC, H_2O 20 %/CH_3CN 80 %, ret. time: 3.7033 min.

4.5.13. N-(4-chlorophenyl)-2-{[(5-chloro-2-thienyl)carbonyl]amino}-5,6,7,8-tetrahydro-4H-cyclohepta[b]thiophene-3-carboxamide (35)

The title compound was prepared starting from **58** [40] through Method C using 5-chlorothiophene-2-carbonyl chloride and purified by crystallization by EtOH/DMF, in 10 % yield as yellow solid. ^{1}H NMR (400 MHz, DMSO-d_6): δ 1.52–1.55 (m, 2H, cycloheptane CH_2), 1.59–1.62 (m, 2H, cycloheptane CH_2), 1.80–1.84 (m, 2H, cycloheptane CH_2), 2.70–2.75 (m, 4H, cycloheptane CH_2), 7.23 (d, $J = 3.28$ Hz, 1H, thiophene CH), 7.38 (d, $J = 8.12$ Hz, 2H, aromatic CH), 7.67 (d, $J = 3.25$

Hz, 1H, thiophene CH), 7.76 (d, J = 8.38 Hz, 2H, aromatic CH), 10.31 and 11.11 (s, each 1H, NH). ^{13}C NMR (101 MHz, DMSO-d_6): δ 27.70, 28.28 (2C), 28.99, 32.33, 121.70, 126.33, 128.89, 128.91, 130.19, 133.07, 133.90, 134.79, 136.60, 137.53, 138.85, 158.21, 163.42. HRMS (ESI) m/z [M − H]$^-$ calcd for $C_{21}H_{18}Cl_2N_2O_2S_2$ 464.01867, found 464.01928. HPLC, H_2O with 0.1 % FA 10 %/CH_3CN 90 %, ret. time: 4.2733 min.

4.5.14. N-(4-chlorophenyl)-2-[(2-methoxy-4-nitrobenzoyl)amino]-5,6,7,8-tetrahydro-4H-cyclohepta[b]thiophene-3-carboxamide (70)

The title compound was prepared starting from **58** [40] through Method C using 2-methoxy-4-nitrobenzoyl chloride and purified by trituration with Et_2O/EtOH, in 47 % yield as yellow solid. ^{1}H NMR (400 MHz, DMSO-d_6): δ 1.59–1.65 (m, 4H, cycloheptane CH_2), 1.81–1.85 (m, 2H, cycloheptane CH_2), 2.75–2.82 (m, 4H, cycloheptane CH_2), 4.06 (s, 3H, OCH_3), 7.43 (d, J = 8.5 Hz, 2H, aromatic CH), 7.80 (d, J = 8.4 Hz, 2H, aromatic CH), 7.95–7.98 (m, 2H, aromatic CH), 8.25 (d, J = 8.8 Hz, 1H, aromatic CH), 10.27 and 11.82 (s, each 1H, NH).

4.5.15. N-(4-chlorophenyl)-2-[(2-hydroxy-4-nitrobenzoyl)amino]-5,6,7,8-tetrahydro-4H-cyclohepta[b]thiophene-3-carboxamide (34)

The title compound was prepared starting from **70** through Method D and purified by crystallization by EtOH/DMF, in 79 % yield as white solid. ^{1}H NMR (400 MHz, DMSO-d_6): δ 1.60–1.65 (m, 4H, cycloheptane CH_2), 1.81–1.86 (m, 2H, cycloheptane CH_2), 2.76–2.80 (m, 4H, cycloheptane CH_2), 7.44 (d, J = 8.7 Hz, 2H, aromatic CH), 7.71–7.80 (m, 4H, aromatic CH), 8.21 (d, J = 8.6 Hz, 1H, aromatic CH), 10.29 and 11.99 (s, each 1H, NH), 12.82 (s, 1H, OH). ^{13}C NMR (101 MHz, DMSO-d_6): δ 27.77, 28.23, 28.95 (2C), 32.30, 111.95, 114.56, 122.14, 123.01, 123.38, 127.96, 129.21, 132.10, 133.17, 135.70, 136.31, 138.21, 150.61, 157.12, 160.32, 164.26. HRMS (ESI) m/z [M − H]$^-$ calcd for $C_{23}H_{20}ClN_3O_5S$ 484.0739 found 484.07318. HPLC, H_2O 30 %/CH_3CN 70 %, ret. time: 6.5733 min.

4.5.16. 2-[(4-Cyanobenzoyl)amino]-N-[4-(trifluoromethyl)phenyl]-5,6,7,8-tetrahydro-4H-cyclohepta[b]thiophene-3-carboxamide (36)

The title compound was prepared starting from **60** [43] through Method C using 4-cyanobenzoyl chloride and purified by crystallization by EtOH/DMF, in 47 % yield as yellow solid. ^{1}H NMR (400 MHz, DMSO-d_6): δ 1.57–1.63 (m, 4H, cycloheptane CH_2), 1.78–1.82 (m, 2H, cycloheptane CH_2), 2.74–2.76 (m, 4H, cycloheptane CH_2), 7.71 (d, J = 8.6 Hz, 2H, aromatic CH), 7.97–8.02 (m, 6H, aromatic CH), 10.60 and 11.29 (s, each 1H, NH). ^{13}C NMR (101 MHz, DMSO-d_6): δ 27.78, 28.40 (2C), 29.03, 32.41, 114.71, 118.74, 120.05, 123.87 (q, J = 32.7 Hz), 125.06 (q, J = 278.76 Hz), 125.73, 126.44, 129.13, 132.87, 133.10, 134.72, 136.58, 137.84, 143.64, 163.47, 163.97. HRMS (ESI) m/z [M + Na]$^+$ calcd for $C_{25}H_{20}F_3N_3O_2S$ 506.11257, found 506.11312. HPLC, H_2O 20 %/CH_3CN 80 %, ret. time: 3.7133 min.

4.5.17. 2-{[(5-Chloro-2-thienyl)carbonyl]amino}-N-[4-(trifluoromethyl)phenyl]-5,6,7,8-tetrahydro-4H-cyclohepta[b]thiophene-3-carboxamide (39)

The title compound was prepared starting from **60** [43] through Method C using 5-chlorothiophene-2-carbonyl chloride and purified by crystallization by EtOH/DMF, in 26 % yield as white solid. ^{1}H NMR (400 MHz, DMSO-d_6): δ 1.53–1.58 (m, 2H, cycloheptane CH_2), 1.60–1.64 (m, 2H, cycloheptane CH_2), 1.80–1.84 (m, 2H, cycloheptane CH_2), 2.71–2.77 (m, 4H, cycloheptane CH_2), 7.23 (d, J = 4.09 Hz, 1H, aromatic CH), 7.68–7.70 (m, 3H, aromatic CH), 7.94 (d, J = 8.50 Hz, 2H, aromatic CH), 10.53 and 11.05 (s, each 1H, NH). ^{13}C NMR (101 MHz, DMSO-d_6): δ 27.68, 28.22, 28.97, 32.32, 32.97, 119.99, 123.73 (q, J=32.3 Hz), 124.99 (q, J=284.8 Hz), 126.08, 126.30 (q, J=3.0 Hz), 128.89, 130.22, 133.12, 134.14, 134.81, 136.61, 137.52, 143.52, 158.25, 163.79. HRMS (ESI) m/z [M − H]$^-$ calcd for $C_{22}H_{18}ClF_3N_2O_2S_2$ 498.04503, found 498.04553. HPLC, RP C18, H_2O with 0.1 % FA 10 %/CH_3CN 90 %, ret. time: 4.1900 min.

4.5.18. 2-[(2-Methoxy-4-nitrobenzoyl)amino]-N-[4-(trifluoromethyl)phenyl]-5,6,7,8-tetrahydro-4H-cyclohepta[b]thiophene-3-carboxamide (71)

The title compound was prepared starting from **60** [43] through Method C using 2 methoxy-4-nitrobenzoyl chloride and purified by trituration with Et_2O/EtOH, in 83 % yield as yellow solid. ^{1}H NMR (400 MHz, DMSO-d_6): δ 1.60–1.66 (m, 4H, cycloheptane CH_2), 1.81–1.85 (m, 2H, cycloheptane CH_2), 2.78–2.83 (m, 4H, cycloheptane CH_2), 4.07 (s. 3H, OCH_3), 7.75 (d, J = 8.4 Hz, 2H, aromatic CH), 7.96–8.00 (m, 4H, aromatic CH), 8.25 (d, J = 8.9 Hz, 1H, aromatic CH), 10.49 and 11.84 (s, each 1H, NH).

4.5.19. 2-(2-Methoxybenzamido)-N-(4-(trifluoromethyl)phenyl)-5,6,7,8-tetrahydro-4H-cyclohepta[b]thiophene-3-carboxamide (72)

The title compound was prepared starting from **60** [43] through Method C using 2-methoxybenzoyl chloride and purified by crystallization by EtOH/DMF, in 39 % yield as brown solid. ^{1}H NMR (400 MHz, DMSO-d_6): δ 1.52–1.68 (m, 4H, cycloheptane CH_2), 1.77–1.81 (m, 2H, cycloheptane CH_2), 2.73–2.81 (m, 4H, cycloheptane CH_2), 3.93 (s, 3H, CH_3), 7.15 (t, J = 7.6 Hz, 1H, aromatic CH), 7.23 (d, J = 8.4 Hz, 1H, aromatic CH), 7.60 (t, J = 7.2 Hz, 1H, aromatic CH), 7.75 and 7.99 (d, J = 8.4 Hz, each 2H. aromatic CH), 8.07 (d, J = 7.3 Hz, 1H, aromatic CH), 10.49 and 11.82 (s, each 1H, NH).

4.5.20. 2-(2-Hydroxybenzamido)-N-(4-(trifluoromethyl)phenyl)-5,6,7,8-tetrahydro-4H-cyclohepta[b]thiophene-3-carboxamide (37)

The title compound was prepared starting from **72** through Method D and purified by crystallization by EtOH, in 80 % yield as yellow solid. ^{1}H NMR (400 MHz, DMSO-d_6): δ 1.53–1.71 (m, 4H, cycloheptane CH_2), 1.79–1.83 (m, 2H, cycloheptane CH_2), 2.71–2.80 (m, 4H, cycloheptane CH_2), 6.93–7.05 (m, 2H, aromatic CH), 7.36–7.43 (m, 1H, aromatic CH), 7.74 and 7.91 (d, J = 7.0 Hz, each 2H, aromatic CH), 7.98 (d, J = 7.1 Hz, 1H, aromatic CH), 10.50 (s, 1H, NH), 11.72 (s, 1H, OH), 11.90 (s, 1H, NH). ^{13}C NMR (101 MHz, DMSO-d_6): δ 27.74, 28.27, 28.92 (2C), 32.24, 117.36, 117.71, 120.31, 120.42 (2C), 122.34, 124.25 (J = 32.3 Hz), 124.96 (J = 272.7 Hz), 126.31, 131.49, 134.36, 135.41, 137.03, 143.01, 156.83, 162.25, 164.74. HRMS (ESI) m/z [M − H]$^-$ calcd $C_{24}H_{21}F_3N_2O_3S$ 473.1152 found 473.11444. HPLC, H_2O 20 %/CH_3CN 80 %, ret. time: 4.3967 min.

4.5.21. 2-[(2-Hydroxy-4-nitrobenzoyl)amino]-N-[4-(trifluoromethyl)phenyl]-5,6,7,8-tetrahydro-4H-cyclohepta[b]thiophene-3-carboxamide (38)

The title compound was prepared starting from **71** through Method D and purified by crystallization by EtOH/DMF, in 21 % yield as white solid. ^{1}H NMR (400 MHz, DMSO-d_6): δ 1.60–1.66 (m, 4H, cycloheptane CH_2), 1.81–1.84 (m, 2H, cycloheptane CH_2), 2.76–2.81 (m, 4H, cycloheptane CH_2), 7.74–7.80 (m, 4H, aromatic CH), 7.91 (d, J = 7.6 Hz, 2H, aromatic CH), 8.21 (d, J = 8.6 Hz, 1H, aromatic CH), 10.52 and 11.99 (s, each 1H, NH), 12.71 (s, 1H, OH). ^{13}C NMR (101 MHz, DMSO-d_6): δ 27.75, 28.22, 28.94 (2C), 32.29, 111.97, 114.58, 120.44, 122.78, 123.39, 123.85 (q, J = 58.6 Hz), 125.37 (q, J = 183.8 Hz), 126.63, 132.19, 133.17, 135.73, 136.66, 142.87, 150.62, 157.13, 160.41, 164.64. HRMS (ESI) m/z [M − H]$^-$ calcd for $C_{24}H_{20}F_3N_3O_5S$ 518.1005 found 518.09986. HPLC, H_2O 20 %/CH_3CN 80 %, ret. time: 3.2833 min.

4.5.22. 2-[(4-Cyanobenzoyl)amino]-N-1,3-thiazol-2-yl-5,6,7,8-tetrahydro-4H-cyclohepta[b]thiophene-3-carboxamide (40)

The title compound was prepared starting from **64** [40] through Method C using 4-cyanobenzoyl chloride and purified by crystallization by EtOH/DMF, in 58 % yield as yellow solid. ^{1}H NMR (400 MHz, DMSO-d_6): δ 1.56–1.62 (m, 4H, cycloheptane CH_2), 1.81–1.87 (m, 2H, cycloheptane CH_2), 2.75–2.82 (m, 4H, cycloheptane CH_2), 7.23 (d, J = 3.2 Hz, 1H, aromatic CH), 7.53 (d, J = 3.7 Hz, 1H, aromatic CH), 8.02–8.06 (m, 4H, aromatic CH), 11.48 and 12.37 (s, each 1H, NH). ^{13}C NMR (101 MHz, DMSO-d_6): δ 27.73, 28.15, 28.35, 29.00, 32.51, 113.59,

114.74, 118.79, 123.25, 129.20, 132.60, 133.18, 137.04, 137.80, 163.15. HRMS (ESI) *m/z* $[M + H]^+$ calcd for $C_{21}H_{18}N_4O_2S_2$ 423.0944, found 423.09504. HPLC, H_2O 30 %/CH_3CN 70 %, ret. time: 4.4433 min.

4.5.23. 2-{[(5-Chloro-2-thienyl)carbonyl]amino}-N-1,3-thiazol-2-yl-5,6,7,8-tetrahydro-4H-cyclohepta[b]thiophene-3-carboxamide (42)

The title compound was prepared starting from **64** [40] through Method C using 5-chlorothiophene-2-carbonyl chloride and purified by crystallization by EtOH/DMF, in 32 % yield as yellow solid. ^{1}H NMR (400 MHz, DMSO-d_6): δ 1.52–1.55 (m, 2H, cycloheptane CH_2), 1.59–1.62 (m, 2H, cycloheptane CH_2), 1.80–1.84 (m, 2H, cycloheptane CH_2), 2.68–2.74 (m, 4H, cycloheptane CH_2), 7.22–7.23 (m, 2H, aromatic CH), 7.51 (d, J = 3.42 Hz, 1H, aromatic CH), 7.71 (d, J = 11.09 Hz, 1H, aromatic CH), 11.50 and 12.32 (s, each 1H, NH). ^{13}C NMR (101 MHz, DMSO-d_6): 27.62, 28.07, 28.21, 28.93, 32.38, 113.48, 123.47, 128.92, 130.28, 132.72, 134.83, 136.96, 137.55, 158.02. HRMS (ESI) *m/z* $[M - H]^-$ calcd for $C_{18}H_{16}ClN_3O_2S_3$ 437.00932, found 437.01073. HPLC, H_2O with 0.1 % FA 10 %/CH_3CN 90 %, ret. time: 3.6300 min.

4.5.24. 2-[(2-Methoxy-4-nitrobenzoyl)amino]-N-1,3-thiazol-2-yl-5,6,7,8-tetrahydro-4H-cyclohepta[b]thiophene-3-carboxamide (73)

The title compound was prepared starting from **64** [40] through Method C using 2-methoxy-4-nitrobenzoyl chloride and purified by trituration with Et_2O/EtOH, in 88 % yield as yellow solid. ^{1}H NMR (400 MHz, DMSO-d_6): δ 1.59–1.64 (m, 4H, cycloheptane CH_2), 1.81–1.85 (m, 2H, cycloheptane CH_2), 2.75–2.78 (m, 2H, cycloheptane CH_2), 2.91–2.94 (m, 2H, cycloheptane CH_2), 4.19 (s, 3H, OCH_3), 7.29 (d, J = 3.5 Hz, 1H, aromatic CH), 8.56 (d, J = 3.6 Hz, 1H, aromatic CH), 7.95–7.98 (m, 2H, aromatic CH), 8.27 (d, J = 8.2 Hz, 1H, aromatic CH), 8.60 and 12.28 (s, each 1H, NH).

4.5.25. 2-[(2-Hydroxy-4-nitrobenzoyl)amino]-N-1,3-thiazol-2-yl-5,6,7,8-tetrahydro-4H-cyclohepta[b]thiophene-3-carboxamide (41)

The title compound was prepared starting from **73** through Method D and purified by crystallization by EtOH/DMF, in 57 % yield as white solid. ^{1}H NMR (400 MHz, DMSO-d_6): δ 1.59–1.64 (m, 4H, cycloheptane CH_2), 1.81–1.85 (m, 2H, cycloheptane CH_2), 2.73–2.77 (m, 2H, cycloheptane CH_2), 2.84–2.86 (m, 2H, cycloheptane CH_2), 6.54 (d, J = 3.5 Hz, 1H, aromatic CH), 7.55 (d, J = 3.4 Hz, 1H, aromatic CH), 7.78–7.82 (m, 2H, aromatic CH), 8.20 (d, J = 8.6 Hz, 1H, aromatic CH), 12.41 (bs, 3H, OH and NH x 2). ^{13}C NMR (101 MHz, DMSO-d_6): δ 27.74, 28.21, 28.74, 28.88, 32.36, 112.07, 113.96, 114.53, 121.21, 123.66, 132.04, 133.13, 136.17, 137.69, 150.59, 157.19, 159.12, 160.55, 162.85, 164.79. HRMS (ESI) *m/z* $[M - H]^-$ calcd for $C_{20}H_{18}N_4O_5S_2$ 459.0792 found 459.07968. HPLC, H_2O 30 %/CH_3CN 70 %, ret. time: 4.3367 min.

4.5.26. 2-[(4-Cyanobenzoyl)amino]-N-(2-methoxyphenyl)-5,6,7,8-tetrahydro-4H-cyclohepta[b]thiophene-3-carboxamide (74)

The title compound was prepared starting from **65** [44] through Method C using 4-cyanobenzoyl chloride and purified by crystallization by EtOH/DMF, in 49 % yield as yellow solid. ^{1}H NMR (400 MHz, DMSO-d_6): δ 1.64–1.65 (m, 4H, cycloheptane CH_2), 1.83–1.86 (m, 2H, cycloheptane CH_2), 2.77–2.79 (m, 2H, cycloheptane CH_2), 2.87–2.90 (m, 2H, cycloheptane CH_2), 3.71 (s, 3H, OCH_3), 6.97 (t, J = 7.5 Hz, 1H, aromatic CH), 7.06 (d, J = 8.3 Hz, 1H, aromatic CH), 7.13 (t, J = 8.0 Hz, 1H, aromatic CH), 8.05–8.10 (m, 5H, aromatic CH), 8.97 and 11.29 (s, each 1H, NH).

4.5.27. 2-(2-Methoxybenzamido)-N-(2-methoxyphenyl)-5,6,7,8-tetrahydro-4H-cyclohepta[b]thiophene-3-carboxamide (75)

The title compound was prepared starting from **65** [44] through Method C using 2-methoxybenzoyl chloride and purified by flash chromatography eluting with cyclohexane/EtOAc (90:10), in 6 % yield as yellow solid. ^{1}H NMR (400 MHz, DMSO-d_6): δ 1.53–1.65 (m, 4H, cycloheptane CH_2), 1.80–1.84 (m, 2H, cycloheptane CH_2), 2.76–2.79 (m, 2H, cycloheptane CH_2), 2.83–2.95 (m, 2H, cycloheptane CH_2), 3.84 (s, 3H, CH_3), 4.05 (s, 3H, CH_3), 7.01 (t, J = 7.6 Hz, 1H, aromatic CH), 7.10–7.19 (m, 3H, aromatic CH), 7.26 (d, J = 7.9 Hz, 1H, aromatic CH), 7.62 (t, J = 8.1 Hz, 1H, aromatic CH), 8.08 (d, J = 7.8 Hz, 1H, aromatic CH), 8.15 (d, J = 6.8 Hz, 1H, aromatic CH), 8.78 and 12.28 (s, each 1H, NH).

4.5.28. 2-[(2-Methoxy-4-nitrobenzoyl)amino]-N-(2-methoxyphenyl)-5,6,7,8-tetrahydro-4H-cyclohepta[b]thiophene-3-carboxamide (76)

The title compound was prepared starting from **65** [44] through Method C using 2-methoxy-4-nitrobenzoyl chloride and purified by crystallization by EtOH/DMF, in 88 % yield as yellow solid. ^{1}H NMR (400 MHz, DMSO-d_6): δ 1.68–1.70 (m, 4H, cycloheptane CH_2), 1.85–1.89 (m, 2H, cycloheptane CH_2), 2.79–2.80 (m, 2H, cycloheptane CH_2), 2.92–2.94 (m, 2H, cycloheptane CH_2), 3.85 and 4.18 (s, each 3H, OCH_3), 7.02–7.06 (m, 1H, aromatic CH), 7.11–7.16 (m, 1H, aromatic CH), 7.39–7.40 (m, 1H, aromatic CH), 7.96–7.99 (m, 2H, aromatic CH), 8.13–8.16 (m, 1H, aromatic CH), 8.29–8.32 (m, 1H, aromatic CH), 8.80 and 12.30 (s, each 1H, NH).

4.5.29. 2-{[(5-Chloro-2-thienyl)carbonyl]amino}-N-(2-methoxyphenyl)-5,6,7,8-tetrahydro-4H-cyclohepta[b]thiophene-3-carboxamide (77)

The title compound was prepared starting from **65** [44] through Method B using 5-chlorothiophene-2-carbonyl chloride without purification, in 65 % yield as yellow solid. ^{1}H NMR (400 MHz, $CDCl_3$): δ 1.76–1.78 (m, 4H, cycloheptane CH_2), 1.94–1.96 (m, 2H, cycloheptane CH_2), 2.81–2.82 (m, 2H, cycloheptane CH_2), 3.00–3.02 (m, 2H, cycloheptane CH_2), 3.94 (s, 3H, CH_3), 6.95–6.99 (m, 2H, aromatic CH), 7.02–7.16 (m, 2H, aromatic CH), 7.54 (d, J = 4.05 Hz, aromatic CH), 8.19 (s, 1H, NH), 8.50 (d, 1H, J = 7.83 Hz, thiophene CH), 12.02 (s, 1H NH).

4.5.30. 2-[(4-Cyanobenzoyl)amino]-N-(2-hydroxyphenyl)-5,6,7,8-tetrahydro-4H-cyclohepta[b]thiophene-3-carboxamide (43)

The title compound was prepared starting from **74** through Method D and purified by crystallization by EtOH/DMF, in 58 % yield as yellow solid. ^{1}H NMR (400 MHz, DMSO-d_6): δ 1.61–1.65 (m, 4H, cycloheptane CH_2), 1.82–1.86 (m, 2H, cycloheptane CH_2), 2.75–2.79 (m, 2H, cycloheptane CH_2), 2.85–2.89 (m, 2H, cycloheptane CH_2), 6.84 (t, J = 6.7 Hz, 1H, aromatic CH), 6.89 (d, J = 7.7 Hz, 1H, aromatic CH), 7.01 (t, J = 6.7 Hz, 1H, aromatic CH), 7.87–7.89 (m, 1H, aromatic CH), 8.04–8.07 (m, 4H, aromatic CH), 9.09, 9.97 and 11.43 (s, each 1H, NH x 2 and OH). ^{13}C NMR (101 MHz, DMSO-d_6): δ 27.63, 28.24, 28.48, 28.93, 32.29, 114.91, 116.01, 118.76, 119.57, 123.35 (2C), 124.92, 125.81, 126.46, 128.94, 133.32, 135.95, 136.30, 137.36, 148.81, 163.11, 163.70. HRMS (ESI) *m/z* $[M - H]^-$ calcd for $C_{24}H_{21}N_3O_3S$ 430.1231 found 430.12282. HPLC, H_2O 20 %/CH_3CN 80 %, ret. time: 2.7200 min.

4.5.31. 2-(2-Hydroxybenzamido)-N-(2-hydroxyphenyl)-5,6,7,8-tetrahydro-4H-cyclohepta[b]thiophene-3-carboxamide (44)

The title compound was prepared starting from **75** through Method D and purified by crystallization by EtOH/DMF, in 40 % yield as white solid. ^{1}H NMR (400 MHz, DMSO-d_6): δ 1.57–1.63 (m, 4H, cycloheptane CH_2), 1.79–1.83 (m, 2H, cycloheptane CH_2), 2.77–2.81 (m, 2H, cycloheptane CH_2), 2.85–2.93 (m, 2H, cycloheptane CH_2), 6.85 (t, J = 7.4 Hz, 1H, aromatic CH), 6.91 (d, J = 8.0 Hz, 1H, aromatic CH), 6.96–7.04 (m, 3H, aromatic CH), 7.42 (t, J = 8.0 Hz, 1H, aromatic CH), 7.84 and 7.98 (d, J = 7.5 Hz, each 1H, aromatic CH), 8.89 (s, 1H, NH), 9.91 and 11.78 (s, each 1H, OH), 12.29 (s, 1H, NH). ^{13}C NMR (101 MHz, DMSO-d_6): δ 27.68, 28.24, 28.78, 28.86, 32.29, 116.12, 117.27, 117.69, 119.54, 120.19, 121.33, 123.37, 125.80, 126.36, 131.54, 131.58, 134.37, 134.79, 138.25, 148.97, 156.94, 162.17, 164.11. HRMS (ESI) *m/z* $[M - H]^-$ calcd for $C_{23}H_{22}N_2O_4S$ 421.1227 found 421.12213. HPLC, H_2O 20 %/CH_3CN 80 %, ret. time: 3.1000 min.

4.5.32. 2-[(2-Hydroxy-4-nitrobenzoyl)amino]-N-(2-hydroxyphenyl)-5,6,7,8-tetrahydro-4H-cyclohepta[b]thiophene-3-carboxamide (45)

The title compound was prepared starting from **76** through Method D and purified by flash chromatography column eluting with $CHCl_3$/MeOH (95/5), in 21 % yield as yellow solid. ^{1}H NMR (400 MHz, DMSO-d_6): δ 1.69–1.73 (m, 4H, cycloheptane CH_2), 1.83–1.86 (m, 2H, cycloheptane CH_2), 2.75–2.78 (m, 2H, cycloheptane CH_2), 2.90–2.93 (m, 2H, cycloheptane CH_2), 6.85 (t, $J = 7.4$ Hz, 1H, aromatic CH), 6.91 (d, $J = 8.0$ Hz, 1H, aromatic CH), 7.03 (t, $J = 7.4$ Hz, 1H, aromatic CH), 7.77–7.83 (m, 3H, aromatic CH), 8.22 (d, $J = 8.5$ Hz, 1H, aromatic CH), 8.91 and 9.90 (s, each 1H, NH). ^{13}C NMR (101 MHz, DMSO-d_6): δ 27.62, 28.17, 28.79, 28.80, 32.11, 111.98, 114.42, 116.26, 119.60, 122.10, 123.36, 123.66, 125.84, 126.40, 132.40, 133.17, 134.98, 137.82, 148.98, 150.72, 157.29, 160.49, 164.10. HRMS (ESI) *m/z* $[M - H]^-$ calcd for $C_{23}H_{21}N_3O_6S$ 466.1078 found 466.10748. HPLC, RP C18, H_2O 20 %/CH_3CN 80 %, ret. time: 2.5933 min.

4.5.33. 2-{[(5-Chloro-2-thienyl)carbonyl]amino}-N-(2-hydroxyphenyl)-5,6,7,8-tetrahydro-4H-cyclohepta[b]thiophene-3-carboxamide (46)

The title compound was prepared starting from **77** through Method D and purified by flash chromatography eluting with CH_2Cl_2 (100 %) in 20 % yield as a yellow solid. ^{1}H NMR (400 MHz, $CDCl_3$): δ 1.65-1.69 (m, 4H, cycloheptane CH_2), 1.88-1.93 (m, 2H, cycloheptane CH_2), 2.81-2.83 (m, 2H, cycloheptane CH_2), 2.87-2.90 (m, 2H, cycloheptane CH_2), 6.85-6.89 (m, 1H, aromatic CH), 6.93 (dd, J=1.15 and J=7.98 Hz, 1H, aromatic CH), 7.05 (dt, J=1.51 and J=7.88 Hz, 1H, aromatic CH), 7.33 (d, $J = 4.08$ Hz, 1H, aromatic CH), 7.77 (d, $J = 4.11$ Hz, 1H, aromatic CH), 7.93 (d, $J = 7.88$ Hz, 1H, aromatic CH), 9.11 (s, 1H, OH), 9.97 and 11.18 (s, each 1H, NH). ^{13}C NMR (101 MHz, DMSO-d_6): δ 27.53, 28.13, 28.33, 28.90, 32.20, 115.92, 119,45, 123.10, 125.63, 125.76, 126.44, 129.02, 130.20, 133.63, 135.00, 135.03, 136.52, 137.17, 148.66, 158.36, 163.41. HRMS (ESI) *m/z* $[M - H]^-$ calcd for $C_{21}H_{19}ClN_2O_3S_2$ 446.05256, found 446,05378. HPLC, H_2O with 0.1 % FA 10 %/CH_3CN 90 %, ret. time: 3.8500 min.

5. Biology

5.1. Anti-IV activity

5.1.1. Compounds and peptide

RBV (1-D-ribofuranosyl-1,2,4-triazole-3-carboxamide) was purchased from Roche. FPV was purchased from MedChemExpress. Each test compound was dissolved in 100 % DMSO. The $PB1_{1-15}$–Tat peptide was synthesized and purified by the Peptide Facility of CRIBI Biotechnology Center (University of Padua, Padua, Italy). This peptide corresponds to the first 15 amino acids of PB1 protein fused to a short sequence of HIV Tat protein (amino acids 47−59), which allows the delivery into the cell [51]. The $PB1_N$ (aa 1–15) peptide was purchased from Proteogenix.

5.1.2. Cells and virus

Madin-Darby canine kidney (MDCK), human A549, and human embryonic kidney (HEK) 293T cell lines were grown in Dulbecco's modified Eagle's medium (DMEM, Life Biotechnologies) supplemented with 10 % (v/v) fetal bovine serum (FBS, Life Technologies) and antibiotics (100 U/mL penicillin and 100 μg/mL streptomycin, Life Technologies). Cells were maintained at 37 °C in a humidified atmosphere with 5 % CO_2. The IAV/PR/8/34 (H1N1) was kindly provided by P. Digard (Roslin Institute, University of Edinburgh, United Kingdom). The IAV/Wisconsin/67/05 and IBV/Malaysia/2506/4 strains were provided by R. Cusinato (Clinical Microbiology and Virology Unit, Padua University Hospital, Italy). The IBV/Lee/40 strain was obtained from W. S. Barclay (Imperial College, London, United Kingdom). The clinical isolate A/Parma/24/09 was kindly provided by I. Donatelli (Istituto Superiore di Sanità, Rome, Italy).

5.1.3. PA-PB1 interaction enzyme-linked immunosorbent assay (ELISA)

The PA−PB1 interaction was detected by a procedure previously described [52,53]. Briefly, 96-well microtiter plates (Nuova Aptaca) were coated with 400 ng of 6His-$PA_{(239-716)}$ for 3 h at 37 °C and then blocked with 2 % BSA (Sigma) in PBS for 1 h at 37 °C. The 6His-$PA_{(239-716)}$ protein was expressed in *E. coli* strain BL21(DE3)pLysS and purified as already described [38]. After washing, 200 ng of GST-$PB1_{(1-25)}$, or GST alone as a control, were added and incubated in the absence or the presence of test compounds at various concentrations O/N at room temperature. *Escherichia coli*-expressed, purified GST and GST-$PB1_{(1-25)}$ proteins were obtained as previously described [38,54]. After washing, the interaction between 6His-$PA_{(239-716)}$ and GST-$PB1_{(1-25)}$ was detected with a horseradish peroxidase-coupled anti-GST monoclonal antibody (GenScript) diluted 1:3000 in PBS supplemented with 2 % FBS. Following washes, the substrate 3,3′,5,5′tetramethylbenzidine (TMB, KPL) was added and absorbance was measured at 450 nm by an ELISA plate reader (MultiSkan FC, ThermoFisher). Values obtained from the samples treated with only DMSO were used to set as 100 % of PA−PB1 interaction.

5.1.4. Cytotoxicity assay

Cytotoxicity of compounds was tested in MDCK, HEK 293T, and A549 cells by the 3-(4,5-dimethylthiazol-2-yl)-2,5-diphenyl tetrazolium bromide (MTT) method, as previously reported [38,55]. Briefly, cells were grown in 96-well plates for 24 h and then treated with serial dilutions of test compounds, or DMSO as a control, in DMEM supplemented with 10 % FBS. After incubation at 37 °C for 48 h, 5 mg/mL of MTT (Sigma) in PBS was added into each well and incubated at 37 °C for further 4 h. Successively, a solubilization solution was added to lyse the cells and incubated O/N at 37 °C. Finally, optical density was read at the wavelength of 570 nm on a microtiter plate reader (MultiSkan FC, ThermoFisher).

5.1.5. Plaque reduction assay (PRA)

The antiviral activity of test compounds against IAV and IBV was tested by PRA as previously described [38]. MDCK cells were seeded at 5×10^5 cells/well into 12-well plates, and incubated at 37 °C for 24 h. The following day, the culture medium was removed and the monolayers were first washed with serum-free DMEM and then infected with the different IAV and IBV strains at 40 PFU/well in DMEM supplemented with 2 μg/mL of TPCK-treated trypsin (Worthington Biochemical Corporation) and 0.14 % BSA and incubated for 1 h at 37 °C. The IV infection was performed in the presence of different concentrations of test compounds or solvent (DMSO) as a control. After virus adsorption, DMEM containing 2 μg/mL of TPCK-treated trypsin, 0.14 % BSA, 1.2 % Avicel, and DMSO or test compounds was added to the cells. At 48 h post-infection, cells were fixed with 4 % formaldehyde and stained with 0.1 % toluidine blue. Viral plaques were counted, and the mean plaque number in the DMSO-treated control was set at 100 %.

5.1.6. Virus yield reduction assay

Virus yield reduction assays were performed similarly to Ref. [56]. Briefly, A549 cells were seeded at a density of 2×10^4 cells per well in 96-well plates and the next day, were infected with IAV/PR/8/34 at multiplicity of infection (MOI) of 0.01 PFU/cell in the presence of various concentrations of test compounds for 1 h at 37 °C. After incubation, the inoculum was removed, and media containing various concentrations of test compounds were added. FPV was included as a positive control. At 24 h post-infection, supernatants were collected and viral titers were determined by titration in fresh MDCK cells as described above. Nonlinear regression analysis and one-way Anova followed by Dunnett's multiple-comparisons test *versus* IAV-infected, DMSO-treated cells were performed with GraphPad Prism version 10.0.

5.1.7. Minireplicon assays

The minireplicon assay was performed as described [38,57], with

some modifications. Briefly, HEK 293T cells (2×10^5 cells per well) were plated into 24-well plates and incubated overnight at 37 °C. The next day, cells were transfected using calcium phosphate co-precipitation method with pcDNA-PB1, pcDNA-PB2, pcDNA-PA, pcDNA-NP plasmids (100 ng/well of each) along with 50 ng/well of the pPolI-Flu-ffLuc reporter plasmid and 50 ng/well of pRL-SV40 plasmid as a transfection control. Transfections were performed in the presence of different concentrations of test compounds or DMSO. RBV and FPV were used as positive controls for inhibition. Cell medium was removed 4 h post-transfection and replaced with DMEM containing the compounds, RBV, FPV, or DMSO. At 24 h post-transfection, cells were harvested, lysed and both firefly and *Renilla* luciferase activity were measured using the Dual Luciferase Assay Kit (Promega). In each experiment, firefly luciferase activity was normalized with that of the *Renilla* luciferase and relative luciferase units (RLU) were obtained. The activity measured in control transfection reactions containing DMSO was set at 100 % of polymerase activity.

5.1.8. Analysis of nuclear accumulation of the PA-PB1 complex

PA-PB1 nuclear translocation assays were performed as reported [32, 38], with some modifications. HEK 293T cells were transiently transfected using Lipofectamine 3000™ (ThermoFisher Scientific) with pcDNA−PA−GFP and pcDNA−PB1 plasmids, in the absence or the presence of compounds **36**, **43**, and **45**, or DMSO as a control. Compounds **43** and **45** were tested at 0.5 μM, whereas compound **36** was tested at 5 μM. At 14 h post transfection, cells were fixed for 20 min with 4 % formaldehyde in PBS. Successively, cells were incubated for 20 min with DRAQ5™ (BioStatus) in PBS and 4 % FBS, mounted using mounting fluid (70 % glycerol in PBS), and imaged using Nikon ECLIPSE Ti confocal microscope equipped with a 63 × oil immersion objective. The nuclear/cytoplasmic ratio (Fn/c) was determined using the Image J 1.62 public domain software (NIH), from single-cell measurements for each of the nuclear (Fn) and cytoplasmic (Fc) fluorescences. Obtained Fn/c ratios were then analyzed by GraphPad Prism 10 with one-way Anova followed by Dunnett's multiple-comparisons test compared to control (DMSO-treated cells).

5.2. Biophysical studies

5.2.1. PA_C expression and purification

To obtain 6His–$PA_{239–716}$ protein, the pET28a–$PA_{239–716}$ plasmid was transformed into *E. coli* strain BL21(DE3)pLysS (Stratagene). Bacteria cells were grown in Luria Bertani (LB) medium containing 50 μg/mL kanamycin until the OD_{600} was 0.8 and then induced by the addition of 0.5 mM isopropyl-β-D-thiogalactopyranoside (IPTG, Sigma-Aldrich) overnight (O/N) at 16 °C. Cells were pelleted, resuspended in 20 mM Tris-HCl pH 8.0, 500 mM NaCl, 500 mM urea, 10 mM β-mercaptoethanol, 25 mM imidazole, 1 mg/mL lysozyme, and complete protease inhibitors (Roche Molecular Biochemicals), and then lysed by two freeze/thaw cycles and by sonication. The lysate was centrifuged at 16,000×*g* for 30 min, and then applied in an FPLC chromatographic system (ÄKTApurifier™ UPC 10, GE Healthcare) to a 1-mL HisTrap™HP column (Cytiva) that had been equilibrated in resuspension buffer. Protein was eluted with 20 mM Tris-HCl pH 8.0, 500 mM NaCl, 500 mM urea, 10 mM β-mercaptoethanol, and 250 mM imidazole. PA_C was then further purified by means of a HiLoad™ 16/600 Superdex™ 75/200 prep grade column (Cytiva) for size exclusion chromatography, and finally dialysed into storage buffer (20 mM Tris-HCl pH 8.0, 150 mM NaCl, 30 % glycerol, 5 mM DTT) using a HiTrap™ Desalting 5-mL column (Cytiva).

5.2.2. Thermal stability analysis

The Prometheus NT.48 instrument (NanoTemper Technologies, GmbH, Munich, Germany) was used to determine the melting temperatures (Tm). Thermal denaturation assays were performed using in 1 μM PA_c alone, as blank reference, or with 10 μM $PB1_N$, as positive control, or with 50 μM of tested ligands, such as compounds **43**, **45**, and **36** in running buffer consisting of 20 mM TRIS-HCl, 150 mM NaCl, pH 8.0, 1 % glycerol, 0.05 % Tween20 (TRIS-GT) enriched with 1 mM DTT and 5 % DMSO. *High Sensitive Capillaries* were filled with about 8 μL of each sample and placed on the sample holder. Excitation power was set at 80 % and a temperature gradient of 2 °C·min^{-1} from 25 to 75 °C was applied. Intrinsic protein fluorescence at 330 and 350 nm was recorded and relative data were processed by *PR.Stability Analysis* v.1.1 software (NanoTemper Technologies).

5.2.3. MicroScale thermophoresis assays

PA_C recombinant protein was fluorescently labelled to lysine residues with dye RED-NT650-NHS 2nd generation supplied by NanoTemper Technologies (NanoTemper Technologies, GmbH, Munich, Germany), using 1:3 protein:dye ratio. Briefly, 100 μL of a 2.0 μM PA_c solution in labeling buffer (130 mM $NaHCO_3$, 50 mM NaCl, 0.05 % Tween20, pH 8.2) was mixed with 100 μL of 6.0 μM RED-NT650-NHS fluorophore in the same buffer and incubated for 30 min at room temperature (RT) in the dark, according to the instructions of the manufacturer. Unbounded fluorophores were removed by size-exclusion chromatography with running buffer consisting of 20 mM TRIS-HCl, 150 mM NaCl, pH 8.0, 0.05 % Tween20 (TRIS-T buffer). Degree of Labeling (DoL) of 0.84 was determined by absorption spectroscopy using PA_c ε of 74,370 M^{-1} cm^{-1} at 280 nm, and red dye ε of 195,000 M^{-1} cm^{-1} at 650 nm. However, fluorophore absorbs light at 280 nm as well, so a correction factor (Fcorr) of 0.04 was applied.

Thermophoretic measurements were performed at constant target concentration with different serial dilutions of each ligand tested, as following described.

- A) 15 nM RED-PA_c *vs* 150 μM $PB1_N$ (3:1 ligand dilution) in TRIS-T buffer enriched of 1 mM DTT;
- B) 20 nM RED-PA_c *vs* 15 μM **45** (2:1 ligand dilution) in TRIS-T buffer enriched of 1 mM DTT and 2 % DMSO;

In each experiment, the samples were incubated before loading into *Premium Capillaries* (NanoTemper Technologies). The capillary tubes were then submitted to a *Cap Scan* analysis of fluorescent emission at RT to check whether each tube contained the same amount of labelled protein, and the presence of protein sticking to capillary walls. Thermophoretic migrations were recorded using Monolith NT.115 device (NanoTemper Technologies) at RT setting LED power at 60 % and medium MST power. Interaction was analyzed in three independent experiments and recorded data were processed *NanoTemper MO.Affinity Analysis v2.3 in DoT (Default on Time)* setting *hot region* between 4/5s regarding experiment A and C; while in *Initial Fluorescence Analysis* mode setting *Phase 1* as default, in experiment B. This different approach in data analysis recorded, was due to fluorescence variation registered during initial *Cap Scan* in presence of compound **45**. Performing SD-test, as suggested by NanoTemper, samples displayed the same amount of fluorescent protein, so, initial emission change could be ascribed to specific interaction between PA_c and molecule **45**.

Confidence value (±) was indicated next to K_d values. Specifically, confidence values define the range where the K_d falls with a 68 % of certainty, as declared by NanoTemper Technologies. Correlated *Signal to Noise* ratio (S/N) allows judging data quality: a value of more than 5 is desirable, while a value of more than 12 corresponds to an excellent assay, as declared by NanoTemper. S/N: 8.7 for $PA_C + PB1_N$ and 30.8 for PA_C + **45**.

5.3. ADME studies

5.3.1. Chemicals

All solvents, reagents and plasma from rats were purchased from Sigma-Aldrich Srl (Milan. Italy). Pooled Male Donors of 20 mg/mL (HLM) were from BD Gentest-Biosciences (San Jose, CA, USA). Milli-Q

quality water (Millipore, Milford, MA, USA) was used. Acetonitrile and formic acid were used for the chromatographic analyses.

5.3.2. Equilibrium solubility in aqueous media

Thermodynamic solubility values were measured in aqueous media (pH = 7) by the shake flask method. One mg of each compound was placed in 1 mL of Milli-Q water and shaken at room temperature for 24 h. The resulting suspension was filtered through a 0.45 μm nylon filter (Sartorius Stedim Biotech, Gottingen, Germany) and the filtrate was analyzed at λ_{max} of each compound by HPLC using a Jasco LC-4000 instrument equipped with a UV–visible Diode Array Jasco MD-4015 (Jasco Corporation, Tokyo, Japan) and a Gemini LC C18 110 Å column, 3 μm, 100 mm × 2 mm (Phenomenex, Torrance, CA, USA). Chromatographic separation was performed using a gradient elution with CH_3CN:H_2O with formic acid 0.1%$_{v/v}$, eluting from 20 to 100 % of CH_3CN in 10 min at 0.5 mL/min. Solubility values were interpolated from calibration curves prepared from concentrated DMSO stock solutions of each compound diluted with Milli-Q water to a final concentration of 10, 50, and 100 μM. As a positive control, a solution of each compound at a known concentration was used.

5.3.3. UV/LC-MS method

For the quantitative analysis was used a UV/LC-MS system. LC analysis was performed by Agilent 1100 LC/MSD VL system (G1946C) (Agilent Technologies, Palo Alto, CA, USA) constituted by a vacuum solvent degassing unit, a binary high-pressure gradient pump, an 1100 series UV detector, and an 1100 MSD model VL benchtop mass spectrometer. The Agilent 1100 series mass spectra detection (MSD) single-quadrupole instrument was equipped with the orthogonal spray API-ES (Agilent Technologies, Palo Alto, CA, USA). Nitrogen was used as nebulizing and drying gas. Chromatographic separation was performed using a Kinetex 5 μm EVO C18 column (100 Å. 150 × 4.6 mm) and gradient elution with a binary solution; eluent A was H_2O, while eluent B consisted of ACN (both eluents were acidified with formic acid 0.1%$_{v/v}$). The analysis started at 5 % of B for 1 min, then rapidly increased up to 95 % of B in 10 min remaining until 19 min; finally, in 1 min came back to the initial conditions. The analysis was performed at a flow rate of 0.6 mL/min. UV detection was monitored at 254 nm. Spectra were acquired over the scan range *m/z* 50–1500 in both positive and negative mode.

5.3.4. Parallel artificial membrane permeability assay (PAMPA)

Donor solutions were prepared by diluting 1:1$_{v/v}$ 1 mM DMSO compound stock solution with phosphate buffer (10 mM PBS, pH 7.4). Filters were coated with 10 μL of a 1%$_{w/v}$ L-α-phosphatidylcholine solution in dodecane. One hundred-fifty μL of donor solution were added to each well of the filter plate, while 300 μL of solution 50 % DMSO in phosphate buffer were added to each well of the acceptor plate. The sandwich was incubated for 5 h at room temperature under gentle shaking. After the incubation time, the plates were separated and samples taken from both receiver and donor sides were analyzed using the UV/LC-MS method. Apparent permeability (Papp) was calculated according to the following equation and permeability values are expressed in cm/s x 10^{-6}:

$$Papp = \frac{Vd^{*}Va}{(Vd+Va)^{*}A^{*}t} - \ln(1-r)$$

Where.

Va and **Vd** are the volumes in the acceptor and donor well (cm^3). respectively
A is the area of the membrane (cm^2)
t is the incubation time (s)
r the ratio between drug concentration in the acceptor and equilibrium concentration of the drug in the total volume (Vd + Va).

Membrane Retention (MR) was calculated according to the following equation:

$$\%\,MR = \frac{r-(D+A)}{C}*100$$

Where.

r is the ratio between drug concentration in the acceptor and equilibrium concentration of the drug in the total volume (Vd + Va)
D and **A** represent the drug concentration in the donor and acceptor compartments. respectively
C is the equilibrium concentration.

5.3.5. Metabolic stability in human liver microsomes (HLM)

Fifty μM of the tested compound in DMSO were incubated at 37 °C for 1 h under shaking in presence of phosphate buffer (10 mM PBS, pH 7.4), human liver microsomes (HLM) (0.2 mg/mL), and an NADPH solution in 48 mM $MgCl_2$ (V_f 500 μL). The metabolizing reactions were stopped by adding 1 mL of cold ACN. The reaction mixtures were then centrifuged and dried under an N_2 flow. Finally, the amount of the parent drug and metabolites were subsequently determined by UV/LC-MS and calculated with Excel. Data were plotted using GraphPad Prism 8.0. Furosemide was used as reference compound [58].

5.3.6. Plasma stability

Each compound stock solution in DMSO at the final concentration of 2 mM was incubated in the presence of plasma (from rat) and HEPES buffer (25 mM, 140 mM NaCl, pH 7.4) at 37 °C under shaking. At selected time points (0, 5, 15, 30, 60, 120, 360, 1440 min), 50 μL of the mix solution were added with cold ACN and centrifuged at 5000 rpm for 10 min. The supernatant was removed and analyzed by UV/LC-MS to monitor the amount of unmodified compound. Data were calculated with Excel and plotted using GraphPad Prism 8.0. Statistical significance was assessed by using Student's *t*-test (unpaired samples). Dasatinib was used as reference compound [59].

Funding

This work was supported by Ministero dell'Istruzione, dell'Università e della Ricerca, Italy: i) PRIN 2017 - cod. 2017BMK8JR (to T. Felicetti, I. Vicenti, M. De Angelis, S. Sabatini, L. Nencioni, E. Dreassi, V. Cecchetti, and S. Massari), ii) PON "Ricerca e innovazione" 2014–2020, Azione IV.4 (tematiche dell'innovazione) - cod. J91B2100320006 (to T. Felicetti), iii) PRIN 2022 - cod. 20223RYYFC and PRIN 2022 PNRR-cod. P20222YKP8 (to A. Loregian); Associazione Italiana per la Ricerca sul Cancro, AIRC, grant IG 2021 - ID. 25899 (to A. Loregian); Fondazione Cassa di Risparmio di Padova e Rovigo-Bando Ricerca Covid-2019 No. 55777 2020.0162 (to A. Loregian); EU funding within the NextGeneration EU-MUR PNRR Extended Partnership initiative on Emerging Infectious Diseases (Project no. PE00000007, INF-ACT) to: i) A. Loregian, L. Nencioni, and I. Vicenti, and ii) O. Tabarrini and S. Massari who were recipient of INF-ACT Cascade Open Call 2023 (COC-1- 2023-CNR).

CRediT authorship contribution statement

Anna Bonomini: Writing – review & editing, Visualization, Validation, Investigation, Formal analysis, Data curation. **Tommaso Felicetti:** Writing – review & editing, Writing – original draft, Visualization, Validation, Investigation, Formal analysis, Data curation. **Martina Pacetti:** Writing – review & editing, Investigation, Formal analysis. **Chiara Bertagnin:** Writing – review & editing, Visualization, Formal analysis, Data curation. **Alice Coletti:** Visualization, Investigation, Formal analysis. **Federica Giammarino:** Investigation, Formal analysis. **Marta De Angelis:** Investigation, Formal analysis. **Federica Poggialini:**

Investigation, Formal analysis. **Antonio Macchiarulo:** Supervision. **Stefano Sabatini:** Investigation. **Beatrice Mercorelli:** Writing – review & editing, Supervision, Formal analysis, Data curation, Conceptualization. **Lucia Nencioni:** Writing – review & editing, Formal analysis. **Ilaria Vicenti:** Writing – review & editing, Formal analysis, Data curation. **Elena Dreassi:** Writing – review & editing, Investigation, Formal analysis, Data curation. **Violetta Cecchetti:** Writing – review & editing, Supervision. **Oriana Tabarrini:** Writing – review & editing, Supervision, Funding acquisition, Conceptualization. **Arianna Loregian:** Writing – review & editing, Supervision, Project administration, Funding acquisition, Data curation, Conceptualization. **Serena Massari:** Writing – review & editing, Writing – original draft, Validation, Supervision, Project administration, Investigation, Funding acquisition, Data curation, Conceptualization.

Declaration of competing interest

The authors declare that they have no known competing financial interests or personal relationships that could have appeared to influence the work reported in this paper.

Data availability

Data will be made available on request.

Abbreviations used

cHTC	cycloheptathiophene-3-carboxamide
DENV	Dengue virus
FPV	favipiravir
HLM	human liver microsomes
HPIV	Human parainfluenza virus
IV	Influenza
NP	nucleoprotein
PA	polymerase acidic
PAMPA	parallel artificial membrane permeation assay
Papp	apparent permeability
PB1	polymerase basic 1
PB2	polymerase basic 2
PPI	protein-protein interaction
PRA	plaque reduction assay
RBV	ribavirin
RdRP	RNA-dependent RNA polymerase
SARS-CoV-2	Severe acute respiratory syndrome coronavirus-2
WNV	West Nile virus

Appendix A. Supplementary data

Supplementary data to this article can be found online at https://doi.org/10.1016/j.ejmech.2024.116737.

References

[1] R.E. Baker, A.S. Mahmud, I.F. Miller, M. Rajeev, F. Rasambainarivo, B.L. Rice, S. Takahashi, A.J. Tatem, C.E. Wagner, L.F. Wang, A. Wesolowski, C.J.E. Metcalf, Infectious disease in an era of global change, Nat. Rev. Microbiol. 20 (2022) 193–205, https://doi.org/10.1038/S41579-021-00639-Z.

[2] G.T. Keusch, J.H. Amuasi, D.E. Anderson, P. Daszak, I. Eckerle, H. Field, M. Koopmans, S.K. Lam, C.G. Das Neves, M. Peiris, S. Perlman, S. Wacharapluesadee, S. Yadana, L. Saif, Pandemic origins and a One Health approach to preparedness and prevention: solutions based on SARS-CoV-2 and other RNA viruses, Proc. Natl. Acad. Sci. U.S.A. 119 (2022) e2202871119, https://doi.org/10.1073/PNAS.2202871119.

[3] A. Loregian, B. Mercorelli, G. Nannetti, C. Compagnin, G. Palù, Antiviral strategies against influenza virus: towards new therapeutic approaches, Cell. Mol. Life Sci. 71 (2014) 3659–3683, https://doi.org/10.1007/S00018-014-1615-2/FIGURES/3.

[4] Y. Ren, Y. Chen, S. Cao, Targeted inhibition of the endonuclease activity of influenza polymerase acidic proteins, Future Med. Chem. 14 (2022) 571–586, https://doi.org/10.4155/FMC-2021-0264.

[5] L. Hou, Y. Zhang, H. Ju, S. Cherukupalli, R. Jia, J. Zhang, B. Huang, A. Loregian, X. Liu, P. Zhan, Contemporary medicinal chemistry strategies for the discovery and optimization of influenza inhibitors targeting vRNP constituent proteins, Acta Pharm. Sin. B 12 (2022) 1805–1824, https://doi.org/10.1016/J.APSB.2021.11.018.

[6] I. Giacchello, F. Musumeci, I. D'Agostino, C. Greco, G. Grossi, S. Schenone, Insights into RNA-dependent RNA polymerase inhibitors as antiinfluenza virus agents, Curr. Med. Chem. 28 (2020) 1068–1090, https://doi.org/10.2174/0929867327666200114115632.

[7] M. Toots, R.K. Plemper, Next-generation direct-acting influenza therapeutics, Transl. Res. 220 (2020) 33–42, https://doi.org/10.1016/j.trsl.2020.01.005.

[8] W. Chen, J. Shao, Z. Ying, Y. Du, Y. Yu, Approaches for discovery of small-molecular antivirals targeting to influenza A virus PB2 subunit, Drug Discov. Today 27 (2022) 1545–1553, https://doi.org/10.1016/J.DRUDIS.2022.02.024.

[9] S. Pathania, R.K. Rawal, P.K. Singh, RdRp (RNA-dependent RNA polymerase): a key target providing anti-virals for the management of various viral diseases, J. Mol. Struct. 1250 (2022) 131756, https://doi.org/10.1016/J.MOLSTRUC.2021.131756.

[10] J.M. Wandzik, T. Kouba, S. Cusack, Structure and function of influenza polymerase, Cold Spring Harb. Perspect. Med. 11 (2020) a038372, https://doi.org/10.1101/cshperspect.a038372.

[11] A.J.W. te Velthuis, J.M. Grimes, E. Fodor, Structural insights into RNA polymerases of negative-sense RNA viruses, Nat. Rev. Microbiol. (2021) 303–318, https://doi.org/10.1038/s41579-020-00501-8, 2021 195 19.

[12] Z. Zhu, E. Fodor, J.R. Keown, A structural understanding of influenza virus genome replication, Trends Microbiol. 31 (2022) 308–319, https://doi.org/10.1016/j.tim.2022.09.015.

[13] E. Fodor, A.J.W.T. Velthuis, Structure and function of the influenza virus transcription and replication machinery, Cold Spring Harb. Perspect. Med. 10 (2020) 1–14, https://doi.org/10.1101/cshperspect.a038398.

[14] E. Takashita, Influenza polymerase inhibitors: mechanisms of action and resistance, Cold Spring Harb. Perspect. Med. 11 (2021) a038687, https://doi.org/10.1101/cshperspect.a038687.

[15] Y. Furuta, B.B. Gowen, K. Takahashi, K. Shiraki, D.F. Smee, D.L. Barnard, Favipiravir (T-705), a novel viral RNA polymerase inhibitor, Antivir. Res. 100 (2013) 446–454, https://doi.org/10.1016/j.antiviral.2013.09.015.

[16] J.C. Jones, B.M. Marathe, C. Lerner, L. Kreis, R. Gasser, P.N.Q. Pascua, I. Najera, E. A. Govorkova, A novel endonuclease inhibitor exhibits broad-spectrum anti-influenza virus activity in Vitro, Antimicrob. Agents Chemother. 60 (2016) 5504–5514, https://doi.org/10.1128/AAC.00888-16.

[17] A.F. Voter, J.L. Keck, Development of protein–protein interaction inhibitors for the treatment of infectious diseases, Adv. Protein Chem. Struct. Biol. 111 (2018) 197–222, https://doi.org/10.1016/bs.apcsb.2017.07.005.

[18] Y. Akhter, R. Hussain, Protein-protein complexes as targets for drug discovery against infectious diseases, Adv. Protein Chem. Struct. Biol. 121 (2020) 237–251, https://doi.org/10.1016/BS.APCSB.2019.11.012.

[19] N. Goodacre, P. Devkota, E. Bae, S. Wuchty, P. Uetz, Protein-protein interactions of human viruses, Semin. Cell Dev. Biol. 99 (2020) 31–39, https://doi.org/10.1016/J.SEMCDB.2018.07.018.

[20] S. Massari, J. Desantis, M.G. Nizi, V. Cecchetti, O. Tabarrini, Inhibition of influenza virus polymerase by interfering with its protein-protein interactions, ACS Infect. Dis. 7 (2021) 1332–1350, https://doi.org/10.1021/acsinfecdis.0c00552.

[21] T. Felicetti, S. Massari, Protein-protein interactions by influenza polymerase subunits as drug targets, Future Med. Chem. 14 (2022) 53–56, https://doi.org/10.4155/FMC-2021-0259.

[22] G. Palù, A. Loregian, Inhibition of herpesvirus and influenza virus replication by blocking polymerase subunit interactions, Antivir. Res. 99 (2013) 318–327, https://doi.org/10.1016/J.ANTIVIRAL.2013.05.014.

[23] T.P. Peacock, C.M. Sheppard, E. Staller, W.S. Barclay, Host determinants of influenza RNA synthesis, Annu. Rev. Virol. 6 (2019) 215–233, https://doi.org/10.1146/annurev-virology-092917-043339.

[24] E. Staller, W.S. Barclay, Host cell factors that interact with influenza virus ribonucleoproteins, Cold Spring Harb. Perspect. Med. 11 (2021) a038307, https://doi.org/10.1101/CSHPERSPECT.A038307.

[25] T. Krischuns, M. Lukarska, N. Naffakh, S. Cusack, Influenza virus RNA-dependent RNA polymerase and the host transcriptional apparatus, Annu. Rev. Biochem. 90 (2021) 321–348, https://doi.org/10.1146/ANNUREV-BIOCHEM-072820-100645.

[26] T. Uehara, F.G. Hayden, K. Kawaguchi, S. Omoto, A.C. Hurt, M.D. De Jong, N. Hirotsu, N. Sugaya, N. Lee, K. Baba, T. Shishido, K. Tsuchiya, S. Portsmouth, H. Kida, The journal of infectious diseases treatment-emergent influenza variant viruses with reduced baloxavir susceptibility: impact on clinical and virologic outcomes in uncomplicated influenza, J. Infect. Dis. 221 (2020) 346–355, https://doi.org/10.1093/infdis/jiz244.

[27] S. Massari, L. Goracci, J. Desantis, O. Tabarrini, Polymerase acidic protein–basic protein 1 (PA–PB1) protein–protein interaction as a target for next-generation anti-influenza therapeutics, J. Med. Chem. 59 (2016) 7699–7718, https://doi.org/10.1021/acs.jmedchem.5b01474.

[28] X. He, J. Zhou, M. Bartlam, R. Zhang, J. Ma, Z. Lou, X. Li, J. Li, A. Joachimiak, Z. Zeng, R. Ge, Z. Rao, Y. Liu, Crystal structure of the polymerase PAC–PB1N complex from an avian influenza H5N1 virus, Nature 454 (2008) 1123–1126, https://doi.org/10.1038/nature07120.

[29] E. Obayashi, H. Yoshida, F. Kawai, N. Shibayama, A. Kawaguchi, K. Nagata, J.R. H. Tame, S.Y. Park, The structural basis for an essential subunit interaction in influenza virus RNA polymerase, Nature 454 (2008) 1127–1131, https://doi.org/10.1038/nature07225.

[30] A. Ghanem, D. Mayer, G. Chase, W. Tegge, R. Frank, G. Kochs, A. Garcia-Sastre, M. Schwemmle, Peptide-Mediated interference with influenza A virus polymerase, J. Virol. 81 (2007) 7801–7804.
[31] K. Wunderlich, M. Juozapaitis, B. Mänz, D. Mayer, V. Götz, A. Zöhner, T. Wolff, M. Schwemmle, A. Martin, Limited compatibility of polymerase subunit interactions in influenza A and B viruses, J. Biol. Chem. 285 (2010) 16704–16712, https://doi.org/10.1074/JBC.M110.102533.
[32] S. Massari, G. Nannetti, J. Desantis, G. Muratore, S. Sabatini, G. Manfroni, B. Mercorelli, V. Cecchetti, G. Palù, G. Cruciani, A. Loregian, L. Goracci, O. Tabarrini, A Broad anti-influenza hybrid small molecule that potently disrupts the interaction of polymerase acidic protein-basic protein 1 (PA-PB1) subunits, J. Med. Chem. 58 (2015) 3830–3842, https://doi.org/10.1021/acs.jmedchem.5b00012.
[33] S. Massari, C. Bertagnin, M.C. Pismataro, A. Donnadio, G. Nannetti, T. Felicetti, S. Di Bona, M.G. Nizi, L. Tensi, G. Manfroni, M.I. Loza, S. Sabatini, V. Cecchetti, J. Brea, L. Goracci, A. Loregian, O. Tabarrini, Synthesis and characterization of 1,2,4-triazolo[1,5-a]pyrimidine-2-carboxamide-based compounds targeting the PA-PB1 interface of influenza A virus polymerase, Eur. J. Med. Chem. 209 (2021) 112944, https://doi.org/10.1016/j.ejmech.2020.112944.
[34] S. Yuan, H. Chu, H. Zhao, K. Zhang, K. Singh, B.K.C. Chow, R.Y.T. Kao, J. Zhou, B.-J. Zheng, Identification of a small-molecule inhibitor of influenza virus via disrupting the subunits interaction of the viral polymerase, Antivir. Res. 125 (2016) 34–42, https://doi.org/10.1016/j.antiviral.2015.11.005.
[35] J. Zhang, Y. Hu, C. Foley, Y. Wang, R. Musharrafieh, S. Xu, Y. Zhang, C. Ma, C. Hulme, J. Wang, Exploring ugi-azide four-component reaction products for broad-spectrum influenza antivirals with a high genetic barrier to drug resistance, Sci. Rep. 8 (2018) 4653, https://doi.org/10.1038/s41598-018-22875-9.
[36] J. Zhang, Y. Hu, N. Wu, J. Wang, Discovery of influenza polymerase PA-PB1 interaction inhibitors using an in vitro split-luciferase complementation-based assay, ACS Chem. Biol. 15 (2020) 74–82, https://doi.org/10.1021/acschembio.9b00552.
[37] S. Mizuta, H. Otaki, T. Ishikawa, J.N. Makau, T. Yamaguchi, T. Fujimoto, N. Takakura, N. Sakauchi, S. Kitamura, H. Nono, R. Nishi, Y. Tanaka, K. Takeda, N. Nishida, K. Watanabe, Lead optimization of influenza virus RNA polymerase inhibitors targeting PA-PB1 interaction, J. Med. Chem. 65 (2022) 369–385, https://doi.org/10.1021/ACS.JMEDCHEM.1C01527.
[38] G. Muratore, L. Goracci, B. Mercorelli, Á. Foeglein, P. Digard, G. Cruciani, G. Palù, A. Loregian, Small molecule inhibitors of influenza A and B viruses that act by disrupting subunit interactions of the viral polymerase, Proc. Natl. Acad. Sci. U.S.A. 109 (2012) 6247–6252, https://doi.org/10.1073/pnas.1119817109.
[39] S. Massari, G. Nannetti, L. Goracci, L. Sancineto, G. Muratore, S. Sabatini, G. Manfroni, B. Mercorelli, V. Cecchetti, M. Facchini, G. Palu, G. Cruciani, A. Loregian, O. Tabarrini, Structural investigation of cycloheptathiophene-3-carboxamide derivatives targeting influenza virus polymerase assembly, J. Med. Chem. 56 (2013) 10118–10131, https://doi.org/10.1021/jm401560v.
[40] J. Desantis, G. Nannetti, S. Massari, M.L. Barreca, G. Manfroni, V. Cecchetti, G. Palù, L. Goracci, A. Loregian, O. Tabarrini, Exploring the cycloheptathiophene-3-carboxamide scaffold to disrupt the interactions of the influenza polymerase subunits and obtain potent anti-influenza activity, Eur. J. Med. Chem. 138 (2017) 128–139, https://doi.org/10.1016/j.ejmech.2017.06.015.
[41] G. Nannetti, S. Massari, B. Mercorelli, C. Bertagnin, J. Desantis, G. Palù, O. Tabarrini, A. Loregian, Potent and broad-spectrum cycloheptathiophene-3-carboxamide compounds that target the PA-PB1 interaction of influenza virus RNA polymerase and possess a high barrier to drug resistance, Antivir. Res. 165 (2019) 55–64, https://doi.org/10.1016/j.antiviral.2019.03.003.
[42] N.Y. Gorobets, B.H. Yousefi, F. Belaj, C.O.O. Kappe, Rapid microwave-assisted solution phase synthesis of substituted 2-pyridone libraries, Tetrahedron 60 (2004) 8633–8644, https://doi.org/10.1016/j.tet.2004.05.100.
[43] E.C. Truong, P.W. Phuan, A.L. Reggi, L. Ferrera, L.J.V. Galietta, S.E. Levy, A. C. Moises, O. Cil, E. Diez-Cecilia, S. Lee, A.S. Verkman, M.O. Anderson, Substituted 2-Acylaminocycloalkylthiophene-3-carboxylic acid arylamides as inhibitors of the calcium-activated chloride channel transmembrane protein 16A (TMEM16A), J. Med. Chem. 60 (2017) 4626–4635, https://doi.org/10.1021/acs.jmedchem.7b00020.
[44] H.R. Roopa, J. Saravanan, S. Mohan, R. Parmesh, Synthesis , Characterization and Anti-fungal Activity of Some Novel Thiosemicarbazides, 4, 2014, pp. 445–456.
[45] R. Cannalire, K.W. Ki Chan, M.S. Burali, C.P. Gwee, S. Wang, A. Astolfi, S. Massari, S. Sabatini, O. Tabarrini, E. Mastrangelo, M.L. Barreca, V. Cecchetti, S. G. Vasudevan, G. Manfroni, Pyridobenzothiazolones exert potent anti-dengue activity by hampering multiple functions of NS5 polymerase, ACS Med. Chem. Lett. 11 (2020) 773–782, https://doi.org/10.1021/acsmedchemlett.9b00619.
[46] C. Bertagnin, L. Messa, M. Pavan, M. Celegato, M. Sturlese, B. Mercorelli, S. Moro, A. Loregian, A small molecule targeting the interaction between human papillomavirus E7 oncoprotein and cellular phosphatase PTPN14 exerts antitumoral activity in cervical cancer cells, Cancer Lett. 571 (2023) 216331, https://doi.org/10.1016/J.CANLET.2023.216331.
[47] M. Celegato, M. Sturlese, V.V. Costa, M. Trevisan, A.S.L. Dias, I.B.S. Passos, C. M. Queiroz-Junior, L. Messa, A. Favaro, S. Moro, M.M. Teixeira, A. Loregian, B. Mercorelli, Small-molecule inhibitor of flaviviral NS3-NS5 interaction with broad-spectrum activity and efficacy in vivo, mBio 14 (2023) e0309722, https://doi.org/10.1128/MBIO.03097-22.
[48] S. Niebling, O. Burastero, J. Bürgi, C. Günther, L.A. Defelipe, S. Sander, E. Gattkowski, R. Anjanappa, M. Wilmanns, S. Springer, H. Tidow, M. García-Alai, FoldAffinity: binding affinities from nDSF experiments, Sci. Rep. (2021) 1–17, https://doi.org/10.1038/s41598-021-88985-z, 2021 111 11.
[49] M. Jerabek-Willemsen, T. André, R. Wanner, H.M. Roth, S. Duhr, P. Baaske, D. Breitsprecher, MicroScale Thermophoresis: interaction analysis and beyond, J. Mol. Struct. 1077 (2014) 101–113, https://doi.org/10.1016/J.MOLSTRUC.2014.03.009.
[50] A. Corona, J. Desantis, S. Massari, S. Distinto, T. Masaoka, S. Sabatini, F. Esposito, G. Manfroni, E. Maccioni, V. Cecchetti, C. Pannecouque, S.F.J. Le Grice, E. Tramontano, O. Tabarrini, Studies on cycloheptathiophene-3-carboxamide derivatives as allosteric HIV-1 ribonuclease H inhibitors, ChemMedChem 11 (2016) 1709–1720, https://doi.org/10.1002/cmdc.201600015.
[51] S. Fawell, J. Seery, Y. Daikh, C. Moore, L.L. Chen, B. Pepinsky, J. Barsoum, Tat-mediated delivery of heterologous proteins into cells, Proc. Natl. Acad. Sci. U.S.A. 91 (1994) 664–668, https://doi.org/10.1073/pnas.91.2.664.
[52] I. D'Agostino, I. Giacchello, G. Nannetti, A.L. Fallacara, D. Deodato, F. Musumeci, G. Grossi, G. Palù, Y. Cau, I.M. Trist, A. Loregian, S. Schenone, M. Botta, Synthesis and biological evaluation of a library of hybrid derivatives as inhibitors of influenza virus PA-PB1 interaction, Eur. J. Med. Chem. 157 (2018) 743–758, https://doi.org/10.1016/J.EJMECH.2018.08.032.
[53] S. Massari, J. Desantis, G. Nannetti, S. Sabatini, S. Tortorella, L. Goracci, V. Cecchetti, A. Loregian, O. Tabarrini, Efficient and regioselective one-step synthesis of 7-aryl-5-methyl- and 5-aryl-7-methyl-2-amino-[1,2,4]triazolo[1,5-a] pyrimidine derivatives, Org. Biomol. Chem. 15 (2017) 7944–7955, https://doi.org/10.1039/c7ob02085f.
[54] A. Loregian, B.A. Appleton, J.M. Hogle, D.M. Coen, Residues of human cytomegalovirus DNA polymerase catalytic subunit UL54 that are necessary and sufficient for interaction with the accessory protein UL44, J. Virol. 78 (2004) 158–167, https://doi.org/10.1128/jvi.78.1.158-167.2004.
[55] B. Mercorelli, A. Luganini, G. Nannetti, O. Tabarrini, G. Palù, G. Gribaudo, A. Loregian, Drug repurposing approach identifies inhibitors of the prototypic viral transcription factor IE2 that block human cytomegalovirus replication, Cell Chem. Biol. 23 (2016) 340–351, https://doi.org/10.1016/J.CHEMBIOL.2015.12.012.
[56] B. Mercorelli, J. Desantis, M. Celegato, A. Bazzacco, L. Siragusa, P. Benedetti, M. Eleuteri, F. Croci, G. Cruciani, L. Goracci, A. Loregian, Discovery of novel SARS-CoV-2 inhibitors targeting the main protease Mpro by virtual screenings and hit optimization, Antivir. Res. 204 (2022) 105350, https://doi.org/10.1016/J.ANTIVIRAL.2022.105350.
[57] G. Muratore, B. Mercorelli, L. Goracci, G. Cruciani, P. Digard, G. Palù, A. Loregian, Human cytomegalovirus inhibitor AL18 also possesses activity against influenza A and B viruses, Antimicrob. Agents Chemother. 56 (2012) 6009–6013, https://doi.org/10.1128/AAC.01219-12.
[58] A. Brai, F. Poggialini, C. Vagaggini, C. Pasqualini, S. Simoni, V. Francardi, E. Dreassi, Tenebrio molitor as a simple and cheap preclinical pharmacokinetic and toxicity model, Int. J. Mol. Sci. 24 (2023) 2296, https://doi.org/10.3390/IJMS24032296.
[59] H.M. Maher, N.Z. Alzoman, S.M. Shehata, N.O. Abanmy, Validated UPLC-MS/MS method for the quantification of dasatinib in plasma: application to pharmacokinetic interaction studies with nutraceuticals in Wistar rats, PLoS One 13 (2018) e0199208, https://doi.org/10.1371/JOURNAL.PONE.0199208.